Final Degree Thesis

Towards Wearable Spectroscopy Bioimpedance Applications

Power Management for a Battery Driven Impedance Meter

By

RAÚL MACÍAS MACÍAS

UNIVERSITY OF BORÅS

SCHOOL OF ENGINEERING

FINAL DEGREE THESIS 30 ECTS, ERASMUS, SWEDEN
ELECTRICAL ENGINEERING SPECIALIZATION IN COMMUNICATIONS & SIGNAL PROCESSING
THESIS Nº 5/2009

Towards Wearable Spectroscopy Bioimpedance Applications: Power Management for a Battery Driven Impedance Meter

Raúl Macías Macías

Master Thesis
Subject Category: Technology. Biomedical Signal Processing
Series Number Communication and Signal Processing

University of Borås
School of Engineering
SE- 501 90 BORÅS
Telephone +46 33 435 4640

Examiner: Fernando Seoane Martínez
Supervisor: Fernando Seoane Martínez
Date: 2009 May 19th

Keyword: Electrical Bioimpedance, Wearable Medical Device, Power Management, Labview, Smart Textiles.

ABSTRACT

In recent years, due to the combination of technological advances in the fields of measurement instrumentation, communications, home-health care and textile-technology the development of medical devices has shifted towards applications of personal healthcare.

There are well known the available solutions for heart rate monitoring successfully provided by Polar and Numetrex. Furthermore new monitoring applications are also investigated. Among these non-invasive monitoring applications, it is possible to find several ones enable by measurements of Electrical Bioimpedance.

Analog Devices has developed the AD5933 Impedance Network Analyzer which facilitates to a large extent the design and implementation of Electrical Bioimpedance Spectrometers in a much reduced space. Such small size allows the development of a fully wearable bioimpedance measurement.

With the development of a Electrical Bioimpedance-enable wearable medical device in focus for personal healthcare monitoring, in this project, the issue of power management has been targeted and a battery-driven Electrical Bioimpedance Spectrometer based in the AD5933 has been implemented. The resulting system has the possibility to operate with a Li-Po battery with a power autonomy over 17 hours.

ACKNOWLEDGEMENTS

En primer lugar me gustaría dedicar este trabajo a mis padres, Nino y Antonia, y a mis abuelos, Franciso e Isabel y Demetrio e Isabel, por el cariño y amor brindados en todos estos años. Gracias también por haberme cuidado, apoyado y educado como lo habéis hecho así como por haber confiado en mí y haberme dejado la libertad de decidir por mí mismo en todo momento.

También me gustaría agradecer a todos mis amigos todos los momentos compartidos, tanto los buenos como los no tan buenos, y el apoyo recibido. Gracias a todos por haberme hecho disfrutar todos estos años y por haberme animado cuando era necesario.

Gracias también a todos los compañeros que he conocido en mi experiencia Erasmus por haberme ayudado a sentirme como en casa y brindarme su amistad desde el primer momento.

También agradecer a Ramon Bragós, y a todo los compañeros del Laboratorio de Instrumentación y Bioingeniería de la UPC, la paciencia y la gran ayuda ofrecida.

Por último, agradecer a mi supervisor, Dr. Fernando Seoane, toda la paciencia que ha tenido conmigo. Gracias por haberme ayudado a conocer un poco más el mundo de la bioingeniería y por haberme facilitado tanto las cosas en mi experiencia Erasmus, tanto a nivel de estudios como a nivel personal.

De corazón, ¡muchas gracias a todos!

Raúl Macías Macías

TABLE OF CONTENTS

LIST OF ACRONYMS

AC	-	Alternating Current
ADC	-	Analog-to-Digital Converter
AFE	-	Analog Front-End
BCM	-	Body Cell Mass
BIA	-	Bioelectrical Impedance Analysis
BIS	-	Bioelectrical Impedance Spectroscopy
BIVA	-	Bioelectrical Impedance Vector Analysis
DAC	-	Digital-to-Analog Converter
DC	-	Direct Current
DDS	-	Direct Digital Synthesizer
DFT	-	Discrete Fourier Transform
DSP	-	Digital Signal Processor
EBI	-	Electrical Bio Impedance
ECF	-	Exta-Cellular Fluid
ECW	-	Extra-Cellular Water
EMB	-	Electrical-bioimpedance Measurement Block
I2C	-	Inter-Integrated Circuit
IC	-	Integrated Circuit
ICW	-	Intra-Cellular Water
IP	-	International Protection
I/O	-	Input/Output
FFM	-	Fat-Free Mass
FM	-	Fat Mass
LiPo	-	Lithium-ion Polymer
LSB	-	Least Significant Bit
MF-BIA	-	Multi- Frequency Bioelectrical Impedance Analysis
MSB	-	Most Significant Bit
NI	-	National Instruments
OVP	-	Over-Voltage Protection
PC	-	Personal Computer
PGA	-	Programmable Gain Amplifier
PMB	-	Power Management Block
PWM	-	Pulse-Width Modulation
SF-BIA	-	Single- Frequency Bioelectrical Impedance Analysis
SMBus	-	System Management Bus
SMD	-	Surface Mount Device
SPI	-	Serial Peripheral Interface
TBW	-	Total Body Water
TUS	-	Tissue Under Study
USB	-	Universal Serial Bus
WMD	-	Wearable Medical Device

CHAPTER 1

INTRODUCTION

1.1. Introduction

New methods and devices are constantly required in medicine. Nowadays, there are two important branches of investigation. On the one hand, new methods as minimally invasive as possible for patients are developed. In this sense, Electrical Bioimpedance (EBI) method has been proved as a good solution. As EBI measurements detect changes in the structure and composition of tissues produced by pathophysiological processes, they are used as tool for the diagnosis of some diseases as well as tool for assessing body composition.

On the other hand, new devices are required to monitor continuously some body parameters. These devices should be as wearable as possible to make patient's life easier.

1.2. Motivation

In recent years, the concern for designing medical devices as comfortable and easy-use as possible has grown. Furthermore, the Electrical Bioimpedance Measurements have been proved to be suitable for assessing body composition and also for monitoring some physiological parameters.

Due to these two facts, an Electrical Bioimpedance device, as wearable as possible, is proposed in this thesis to monitoring some body parameters minimizing complications in patients' life.

1.3. Goal

The main goal of this thesis is to design and to implement two modules which will be part of a future wearable medical device. These two modules are the power management block and the impedance converter block. The first one chooses the power source and charges the battery when this is not completely full. The second module target is to measure the load impedance which exists between the input and output pins of the IC manufactured by Analog Devices called AD5933.

Due to this IC uses the I2C communication protocol, a secondary aim is to develop a Labview program to communicate the system with a Master Device and to configure the impedance converter.

1.4. Work done

As previously mentioned, the main aim of this project has been the design and the development of a wearable medical device based on EBI measurements. To reach this, the following tasks have been done:

· Both modules, which are part of the system, were designed by the software called OrCAD. They were designed using Surface Mount Devices (SMDs) to make the design as small and light as possible.

· The designed board was implemented by an external company. Later, all SMDs were soldered by hand on the board.

· After checking the board worked, a program was implemented in a PC by the software called Labview to configure the on-board IC called AD5933 using the I2C protocol.

· Finally, when everything worked, some measurements were acquired to check some board features such as battery life or work range.

1.5. Structure of the Thesis Report

The thesis report is organized in five chapters, appendices and references. Chapter 1 is the introduction part of the thesis. Chapter 2 gives a brief background of Electrical Bioimpedance (EBI) and its application in Measurements of Body Composition, also known as Bioelectrical Impedance Analysis (BIA). Furthermore, Chapter 2 gives a brief idea about using EBI in wearable devices. Chapter 3 explains the on-board designed system using OrCAD. Also, in this chapter the Labview developed software for I2C communication is described. Chapter 4 shows some measurement results; it includes some electrical features of the board and measurements validation. Finally, Chapter 4 is followed by the conclusions and proposed future work in the last chapter.

1.6. Out of Scope

The following points have been decided to leave out of this thesis work:

* The implementation of an Analog Front-End to enable 4-electrod method for biomedical applications has been left out because there was other project to this one.
* To implement an embedded system is out of scope because there is a future proposal where the Analog Front-End module, a Bluetooth module and our two modules, the Power Management module and the Impedance Converter module, should be joined and controlled by a microchip.

CHAPTER 2

BACKGROUND

In biomedical engineering, EBI is a term used to describe the response of a living organism to an externally applied electric current. It is a measure of the opposition to the flow of electric current through the tissues.

The measurement of EBI of humans and animals has proved useful as a diagnosis and monitoring tool for several applications such as respiration rate, impedance cardiography or body composition, known as bioelectrical impedance analysis or simply BIA.(Seoane, 2007)

2.1. Bioimpedance (EBI)

2.1.1. Electrical Properties of Tissue [1]

The electrical properties of biological tissue are determined by its constituents. Any tissue is formed by extracellular fluid and cells. The extracellular fluid (ECF) usually denotes all body fluid outside of cells. This medium which is surrounding the cells contains proteins and ions and it can be divided into plasma (20% of ECF) and interstitial fluid (80% of ECF).

On the other hand, the cell is constituted by a lipid bi-layer plasma membrane. Inside this cell membrane, the cell contains intracellular fluid, also known as cytosol, organelles and the nucleus of the cell.

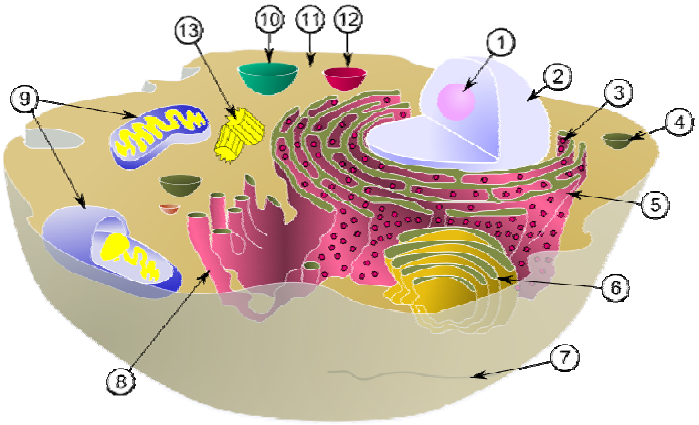

Fig.2.1. A living cell and its constituents: (1) nucleolus, (2) nucleus, (3) ribosome, (4) vesicle, (5) rough endoplasmic reticulum, (6) Golgi apparatus, (7) Cytoskeleton, (8) smooth endoplasmic reticulum, (9) mitochondria, (10) vacuole, (11) cytoplasm, (12) lysosome, (13) centrioles. [2]

Due to free ions contained into extracellular and intracellular fluid, any biological tissue can be considered an electrolyte. An electrolyte can be defined as [3]:

"Any substance that will dissociate into ions in solution and acquire the capacity to conduct electric current in the presence of an external electrical field."

Thus biological tissue is also considered an ionic conductor where K^+, Na^+ and Ca^{2+} are the most important ions contributing to the ionic current.

TABLE 2-I: APPROXIMATE CONCENTRATION OF IONS IN LIVING TISSUE

Important cellular ionic concentrations		
	Intracellular	**Extracellular**
Na^+	10-20 mM	150 mM
K^+	100 mM	5 mM
Ca^{2+}	10(-4) mM	1 mM

As well as having conductance properties, any biological tissue has also dielectric properties. A dielectric can be defined as any material with the ability to store capacitive energy. Although this ability is owned by living tissue at any level due to its constituents, the cellular structure with the major contribution to the dielectric behaviour is the plasma membrane. This membrane is a lipid bi-layer structure with a very poor intrinsic electrical conductance.

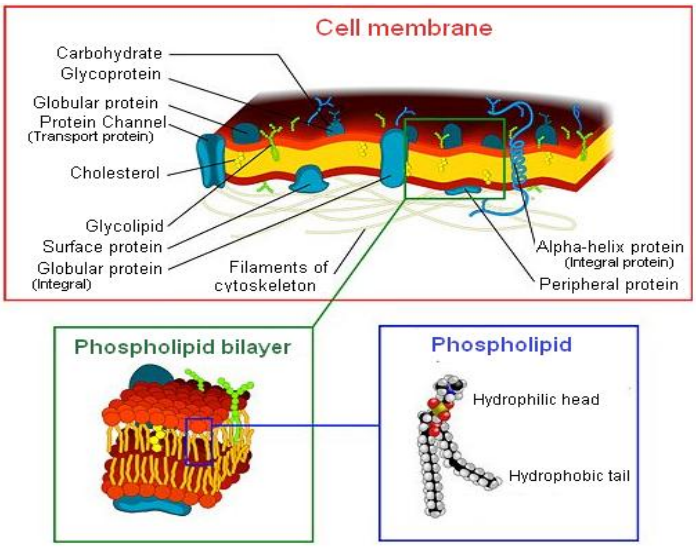

Fig.2.2. Plasma membrane and its structure. [4]

Therefore, the structure formed by the intracellular fluid, plasma membrane and extracellular fluid (conductor-dielectric-conductor) behaves as a capacitor with a specific capacitance of 1 $\mu F/cm^2$.

2.1.2. Tissue as Dispersive Medium [1]

Living tissue is considered as a dispersive medium because of both permittivity and conductivity are functions of frequency. (H.P. Schwan 1957) identified and named three major dispersions: α-, β-, and γ-dispersion. Later (H. P. Schwan 1994) identified a forth dispersion and named δ-dispersion; See Figure 2.3.

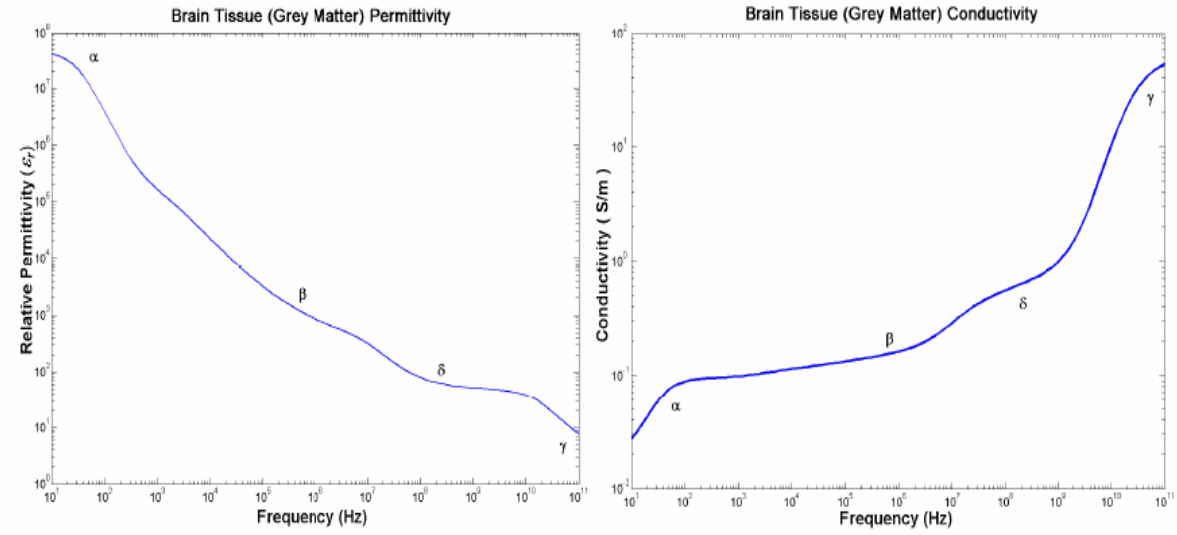

Fig.2.3. Frequency dependence of the conductivity (a) and permittivity (b) in the brain grey matter.

2.1.2.1. α-dispersion

The α-dispersion happens at low frequencies, 10 Hz – 10 kHz. Although all elements which contribute to this frequency dependence are not clearly identified yet, (H.P. Schwan & S. Takashima 1993) established three main causes. First, the effect of the endoplasmic reticulum contributes to this frequency dependence. Second, the channel proteins present in the plasma membrane causes also the frequency-dependent conductance. Finally, the relaxation of counter-ions on the charged cellular surface is another mechanism that produces this frequency dependence.

2.1.2.2. β-dispersion

(Ivorra 2003) established the range of β-dispersion from approximately 10 kHz to 100 kHz. It is caused by the low conductivity and capacitivity properties of the cell membrane and other internal membrane structures and their interactions with the extra and intra-cellular electrolytes.

2.1.2.3. γ-dispersion

This dispersion is due to the high content of water in cell and tissue. Its relaxation frequency is nearly about 20 GHz, like normal water, and its range of dispersion is from hundreds of MHz to some GHz.

2.1.2.4. δ-dispersion

This dispersion is a weak relaxation between β-, and γ-dispersion. It occurs from around 300 MHz to around 2 GHz. This dispersion is caused by rotation of amino acids, partial rotation of charge side groups of proteins, and proteins bonded to water.

The main and more interesting dispersions in medical applications are α- and β-dispersions. In these range is where most changes between pathological and normal tissue occur (Blad B. 1996 Nov).

Finally, in the Table 2-II the four dispersion windows and the elements that contribute to each one are shown.

TABLE 2-II: ELECTRICAL DISPERSIONS OF BIOLOGICAL MATTER*.

Contributing Biomaterial Element		Dispersion			
		α	β	γ	δ
Water and Electrolytes				●	
Biological Macromolecules	Amino acids		●	●	●
	Proteins		●	●	●
	Nucleic acids	●	●	●	●
Vesicles	Surface Charged	●	●		
	Non-Surface Charged		●		
Cells with Membrane	+ Fluids free of protein		●		
	+ Tubular system	●	●		
	+ Surface charge	●	●		
	+ Membrane relaxation	●	●		
	+ Organelles		●	●	●
	+ Protein		●	●	●

*Table contents from (H. P. Schwan 1994)

2.1.3. Electrical Model of Cells

As previously mentioned, electrical properties of tissue are caused by its constituents. Therefore considering these constituents and applying theory of electrical circuits, an explanatory and descriptive electrical model for the cell can be deduced (Fricke 1924); see Figure 2.4

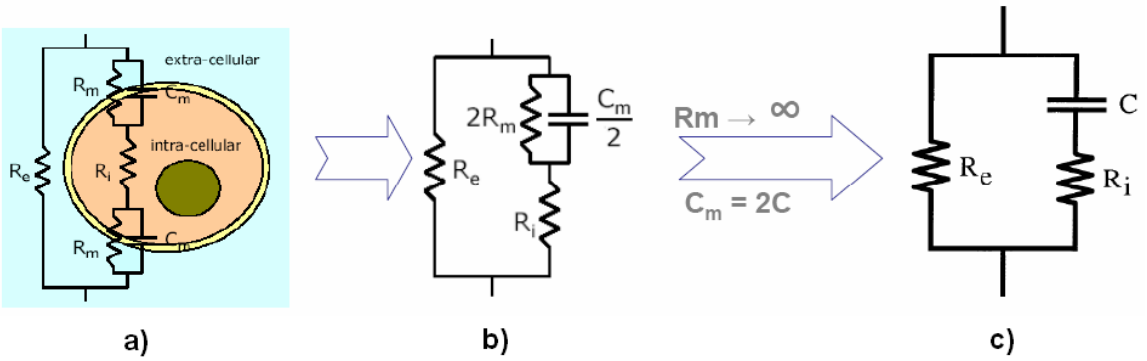

Fig.2.4. Equivalent circuit of a cell where R_e is the extracellular fluid Resistance, R_i is the intracellular fluid Resistance, R_m is the trans-membrane ionic channel Resistance and C_m represents the cell membrane Capacitance.

Usually, as the membrane conductance is very low, the effect of $\mathbf{R_m}$ is neglected and the equivalent electric circuit is very simple (Figure.2.4.c.). According to this simplified model, a frequency dependence introduced by the capacitor **C** exists in biological tissues (Grimmes 2006). It can be observed as at low frequencies, near DC, the current is not able to penetrate the cell because of the plasma membrane acts as an insulator. Therefore, the measured impedance is only the extracellular fluid resistance, $\mathbf{R_e}$. At high frequencies, above 1 MHz, the insulator effect of the plasma membrane decreases and the current flows through the intra and the extracellular fluid. Thus, the measured impedance becomes in the parallel between the intra and the extracellular fluid resistance, $\mathbf{R_i} \,||\, \mathbf{R_e}$.

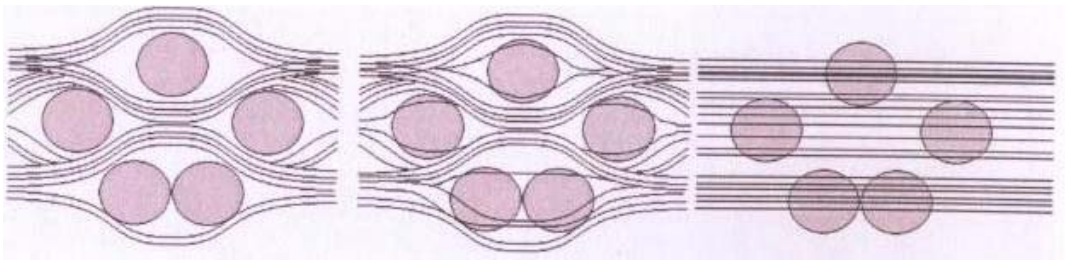

Fig.2.5. Current paths in a suspension of cells at several frequencies.

Attending to the equivalent circuit obtained, the equivalent impedance, which is a complex value, is easily got.

$$Z = R_e \left\| \left(R_i + \frac{1}{j\omega C} \right) = \frac{R_e\left(1 + j\omega C R_i\right)}{1 + j\omega C\left(R_e + R_i\right)} = R + jX \right. \qquad \textbf{Equation (2.1)}$$

Where **Z** is complex impedance [Ω], **R** is the real component or resistance [Ω], **j** is the imaginary unit, and **X** is the imaginary component or reactance [Ω].
And also, the frequency dependence is easily checked.

$$\omega \to 0 \Rightarrow Z_0 = R_e \qquad \textbf{Equation (2.2)}$$

$$\omega \to \infty \Rightarrow Z_\infty = R_e \| R_i = \frac{R_e R_i}{R_e + R_i}$$ **Equation (2.3)**

The validity of Fricke model for tissues and blood was checked by (Kanai 1983), but it was just correct for blood because it contains one dominant cell species (Jaffrin 1997). As human tissue contains different types of cells, the Cole impedance model was proposed by (K. S. Cole 1940) as a more realistic model for tissue. This model consists of three parts: an equation, an equivalent circuit, and a complex impedance circular arc. [5]
The Cole empirical equation for the frequency dependence of tissue or cell suspension complex impedance is

$$Z = R_\infty + \frac{R_0 - R_\infty}{1 + (j\omega\tau)^\alpha}$$ **Equation (2.4)**

Where **Z** is complex impedance [Ω], $\mathbf{R}_\infty$ is the resistance [Ω] at very high frequencies, **j** is the imaginary unit, $\mathbf{R_0}$ is the resistance [Ω] at very low frequencies, **ω** is the angular frequency [1/s], **τ** is the characteristic relaxation time constant of the system [s], and **α** is an exponent [dimensionless] with value 1 as a typical value (single-dispersion).
And its equivalent electrical model is based upon the replacement of the ideal capacitor in the Debye model, shown in the Fig.2.6, with a more general constant phase element (CPE).

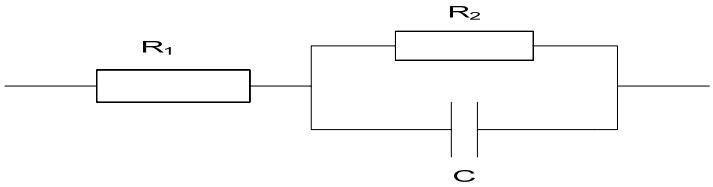

Fig.2.6. Debye single-dispersion electrical model for tissues.

Relating the empirical equation, Equation (2.4), to this model, Fig.2.6, $R_0 = R_1 + R_2$, $R_\infty = R_1$ and $\tau = R_2C$.
Finally, as impedance is a complex magnitude, in the Cole plot its real value (R) is plotted versus its imaginary component, or reactance, (X) with the frequency as a parameter. Thus, the Cole plot is a semicircle with approximated radius $(R_0 - R_\infty)/2$ which crosses the real axis at R_0 and R_∞. The centre of the semicircle is not necessarily in the real axis but beneath it; see Figure 2.7.

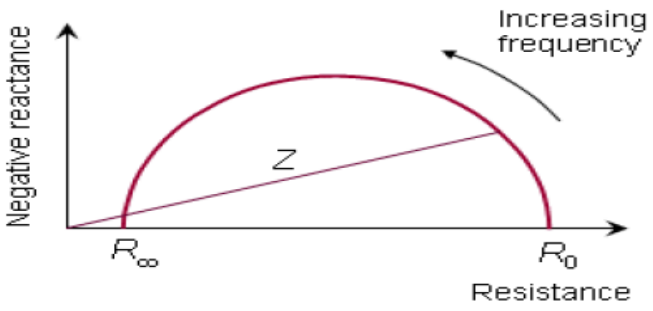

Fig.2.7. Cole plot.

2.2. Body Composition & Bioimpedance Analysis (BIA)

2.2.1. Body Composition Compartments [6]

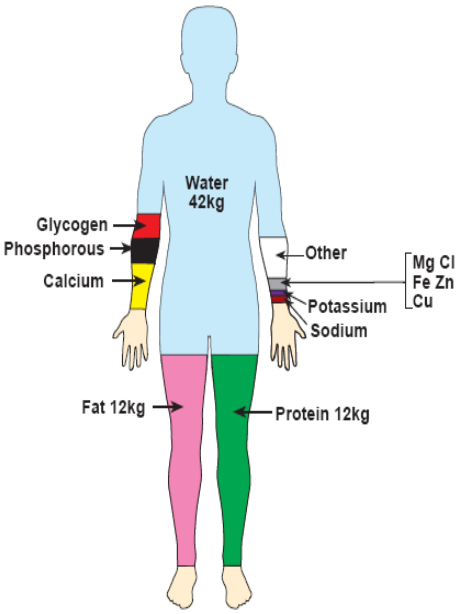

Fig.2.8. Body Composition of a normal weight male. [7]

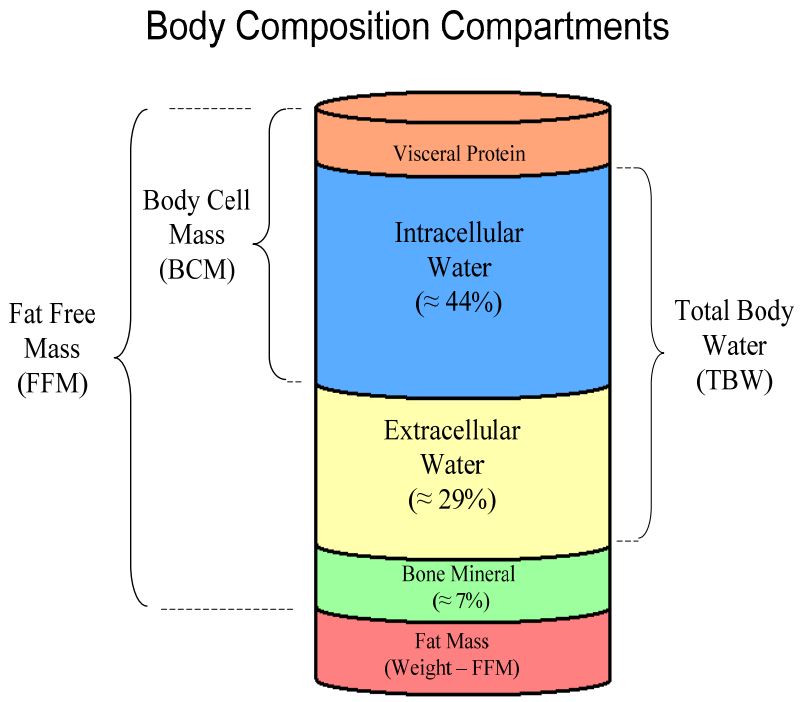

Fig.2.9. Schematic diagram of fat-free mass (FFM), total body water (TBW), intracellular water (ICW), extracellular water (ECW) and body cell mass (BCM).

Fig.2.8 shows the body composition of a hypothetical, normal weight adult. It can be seen that the major component of the human body is water. The protein and fat component are relatively small, with the remainder being primarily bone and minerals. All these components are usually grouped into different compartments; see Fig.2.9.

2.2.1.1. Fat Free Mass (FFM)

The non-fat component of body composition is termed fat free mass, or also lean body mass, and exists primarily as the chief structural and functional component of the human body. This compartment consists in proportions of water (72%), protein (21%) and bone minerals (7%).

2.2.1.2. Total Body Water (TBW)

All of the water content of the human body is termed total body water and it can be divided into intra (ICW) and extracellular water (ECW). TBW usually represents around 60% of the body weight but this can vary between 45 and 75% due to primarily to differences in body fat. It is a measure for evaluating basic hydration status.

2.2.1.3. Intracellular Water (ICW)

All of the water content inside the cells is termed intracellular water and it represents around 2/3 of the TBW.

2.2.1.4. Extracellular Water (ECW)

All of the water outside the cells is termed extracellular water and it represents around 1/3 of TBW.

2.2.1.5. Fat Mass (FM)

Fat mass (FM) is all the extractable lipids from adipose and other tissue in the body. It is the total amount of stored lipids, or fats, in the body and consists of subcutaneous fat and visceral fat. Subcutaneous fat is located directly beneath the skin and serves as an energy reserve and as insulation against outside cold. Visceral fat is located deeper within the body and serves as an energy reserve and as a cushion between organs [8]. It is usually determined as Weight minus FFM.

Due to adipose tissue only contains around 10-15% of water and lean, or muscle, contains around 75% of it, an obese person will have less TBW than a sportsman; see Table 2-III.

TABLE 2-III: COMPOSITION OF AN OBESE MALE & A LEAN MALE.

	Lean Man 70 kg	**Obese Man 100 kg**
Water	60%	47%
Protein	17%	13%
Fat	17%	35%
Remainder	6%	5%

2.2.2. Introduction to BIA [6]

Bioelectrical impedance analysis (BIA) is a method which measures the impedance or opposition to the flow of an electric current through the body fluids contained mainly in the lean and fat tissue [9]. Due to the impedance in lean tissue, where intracellular fluid and electrolytes are primarily contained, is lower than in fat tissue and because of the measured body resistance differs depending on the amount of body fluids, it is possible to estimate the body composition [10]. To achieve it, the body is assumed like a cylinder.

The impedance of a volume conductor is obtained depends on the electrical properties of the material and the shape and orientation respect the Electrical Field. In the case of a cylindrical volume, the resistance of a length of homogeneous conductive material of uniform cross-sectional area is proportional to its length and inversely proportional to its cross sectional area; see Fig.2.10.

$$R = \rho \frac{L}{A}$$ **Equation (2.5)**

Where **R** is the resistance, **ρ** is the resistivity, **L** is the length of the cylinder, and **A** is the cylinder cross sectional area.

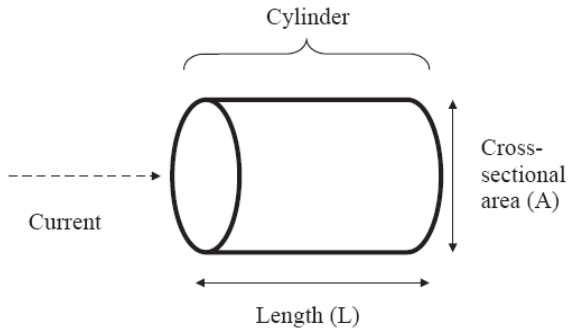

Fig.2.10. Cylinder model for the relationship between the impedance and geometry.

Although the body is not a uniform cylinder and its conductivity/resistivity is not constant, a relationship between the volume of body water and the ratio length^2 to resistance (impedance) can be established as

$$V = \rho \frac{L^2}{R}$$ **Equation (2.6)**

Where **R** is the resistance of the body, **ρ** is the resistivity, **L** is the conductive length, and **V** is the volume of water, which contains electrolytes that conduct the electrical current through the body.
As measuring height is easier than measuring the conductive length [11], which is usually from wrist to ankle, the Equation (2.6) can be modified

$$TBW = k \frac{Ht^2}{R}$$ **Equation (2.7)**

Where **TBW** is Total Body Water, **Ht** is the height, **R** is the resistance of the body, or segment, and **k** is a coefficient which matches the ideal cylinder to the real geometry. The value of this coefficient, **k**, depends on several factors such as sex, age, weight or other anthropometric parameters.

2.2.3. Methods of BIA [6]

2.2.3.1. Single Frequency BIA (SF-BIA)

A single frequency, generally at 50 kHz, is passed between surface electrodes placed on hand and foot (Fig.2.11). At 50 kHz BIA is not strictly measuring TBW but a weighted sum of ECW and ICW. SF-BIA permits to estimate FFM and TBW, but cannot determine differences in ICW and its results are based on a mixture theories and empirical equations.

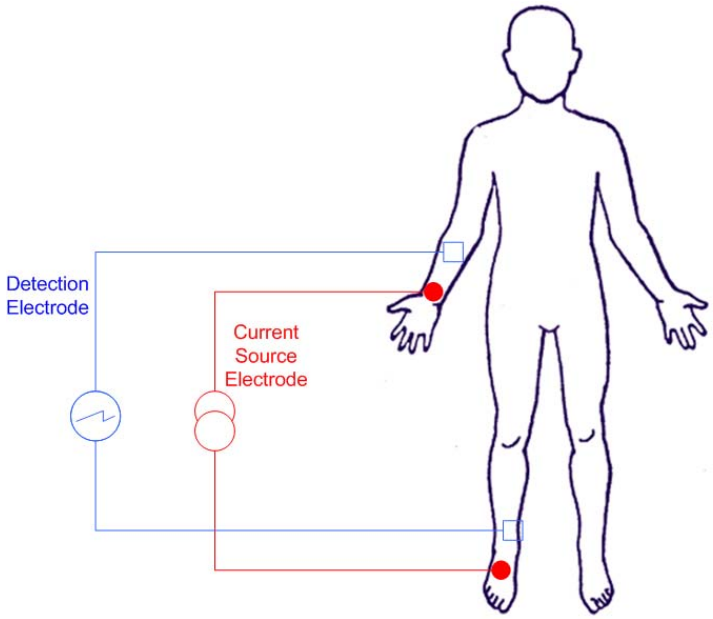

Fig.2.11. Standard placement of electrodes on hand and wrist and foot and ankle for tetrapolar SF-BIA and MF-BIA.

Finally, although SF-BIA is not valid under conditions of significantly altered hydration, it is useful to predict absolute FFM or TBW in normally hydrated subjects.

2.2.3.2. Multi-Frequency BIA (MF-BIA)

MF-BIA, as SF-BIA, uses also empirical linear regression models but includes impedances at multiple frequencies, between 0 and 500kHz, to evaluate FFM, TBW, ICW and ECW. According to (Patel et al.), MF-BIA is more accurate and less biased than SF-BIA for the prediction of ECW but it is less accurate and more biased for TBW.

2.2.3.3. Bioelectrical Spectroscopy (BIS)

In contrast to MF-BIA, BIS uses mathematical modeling and mixture equations, e.g. Cole–Cole plot and Hanai equations (Equation (2.8), (2.9) and (2.10)), to generate relationships between impedance and body fluid compartments or to predict R_0 and R_∞ and then develop empirically derived prediction equations rather than go to mixture modeling. Although BIS models, constants and equations generated in healthy populations have shown to be accurate, the potential of BIS can only be exhausted if the data are interpreted with adequate algorithm that include reliable data fitting and a valid fluid distribution model.

$$V_{ECW} = \sqrt{\left(K_b \rho_{ECW} \frac{H^2}{R_0}\right)^3} \cdot \sqrt[3]{V_b} \qquad \textbf{Equation (2.8)}$$

$$\sqrt[5]{\left(1+\frac{V_{ICW}}{V_{ECW}}\right)^2}=\frac{R_0}{R_\infty}\left(1+K_b\frac{V_{ICW}}{V_{ECW}}\right) \qquad \textbf{Equation (2.9)}$$

$$V_{TBW}=V_{ICW}+V_{ECW} \qquad \textbf{Equation (2.10)}$$

Where $\mathbf{V_x}$ is the volume of the X-compartment, $\boldsymbol{\rho}$ is the resistivity, **H** is body height, $\mathbf{V_b}$ is body volume, $\mathbf{R_0}$ and $\mathbf{R_\infty}$ are the Cole-resistances at low and high frequencies, respectively, and $\mathbf{K_b}$ is a dimensionless shape factor.

2.2.3.4. Segmental-BIA

Segmental-BIA is performed by either placing two additional electrodes on wrist and foot on the opposite side, or by placing sensor electrodes on wrist, shoulder, upper iliac spine and ankle, or by placing electrodes on proximal portion of the forearm and the lower leg and trunk electrode on the shoulder and the upper thigh.

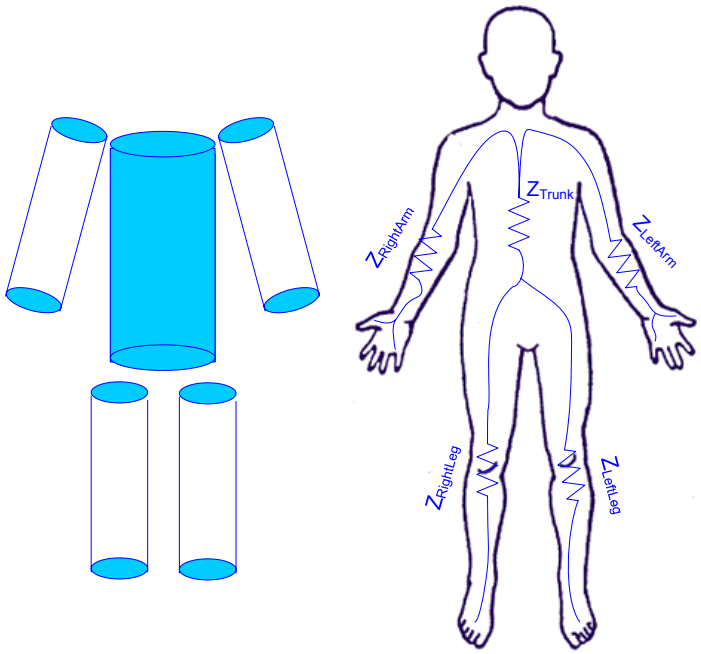

Fig.2.12. Five-Cylinder model of the body and the impedance for each segment: right arm, right leg, left arm, left leg, and trunk.

Although the trunk of the body represents as much as 50% of whole body mass, it only contributes around 10% to whole body impedance. This implies three aspects for body composition analysis by the whole body (one cylinder) BIA approach:

- ❖ Changes of the impedance are closely related to changes of the FFM of the limbs.
- ❖ Changes of the FFM of the trunk are probably not adequately described by whole body impedance measurements.

❖ Even large changes in the fluid volume within the abdominal cavity have only minor influence on the measurement of FFM or BCM.

2.2.3.5. Localized BIA

Due to whole body BIA measures various body segments and is influenced by a several number of effects such as hydration, fat fraction or geometrical boundary conditions, the validity of simple empirical regression models is population-specific. Hence, to minimize the interference effects, Localized BIA, which focuses on well-defined body segments, is used.

2.2.3.6. Bioelectrical Impedance Vector Analysis (BIVA) [12]

BIVA is a new method for monitoring body fluid variation and body analysis developed by (Piccoli et al., 1994). In contrast to other EBI methods, BIVA method is only affected by the impedance measurement error and the biological variability of subjects. Thus, BIA becomes a stand-alone procedure that permits patient evaluation from the direct measurement of the impedance vector and does not depend on equations or models or assumptions about body geometry.

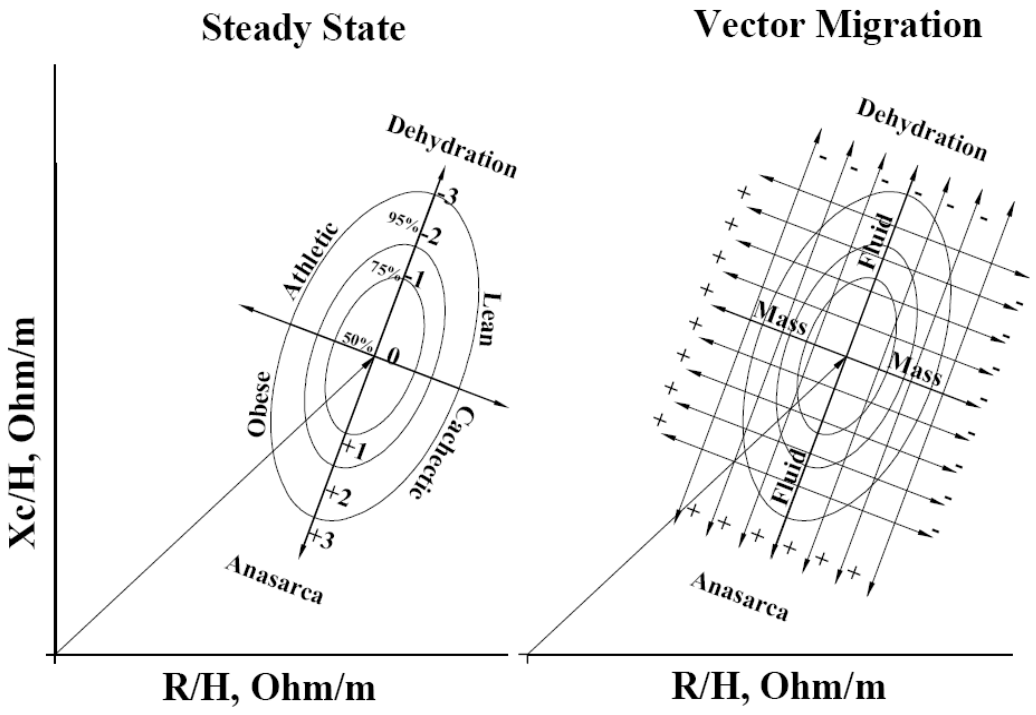

Fig.2.13. BIVA Pattern (RX_c-graph) (Piccoli et al 1994).

In BIVA, Z can be considered as a bivariate random vector: resistance (R) and reactance (X_c). These two variables, standardized for height, are plotted as point vectors in the R–X_c plane. An individual vector can then be compared with the reference 50%, 75%, and 95% tolerance ellipses calculated in the healthy population of the same gender and race. That is called R–X_c graph method; see Fig.2.13. The ellipse varies with age and body size.

Furthermore, the following interpretations can be done when vector falls outside the 75% tolerance ellipse:

- ❖ Vector displacements parallel to the major axis of tolerance ellipses indicate progressive changes in tissue hydration: dehydration with long vectors, out of the upper pole, and hyperhydration, or anasarca, with short vectors, out of the lower pole.
- ❖ Vectors falling above (left) or below (right) the major axis of tolerance ellipses indicate more or less BCM, respectively, contained in lean body tissues.

2.3. Electrodes & EBI Measurement [1]

2.3.1. Introduction to Skin-Electrode Interface

As previously mentioned, EBI does not produce energy by itself. Thus, to measure EBI is needed an externally applied source. The most common EBI measurement method consists on injecting a known electric current and to measure its complementary magnitude, voltage. Therefore, the impedance value can be obtained by the Ohm's law.

$$Z = \frac{V}{I} \qquad \textbf{Equation (2.11)}$$

Where **Z** is the impedance [Ω], **V** is the measured voltage [V], and **I** is the known injected current [A].

Then, to inject the current and to measure the voltage, a device is used. This device which plays both roles is called electrode. Furthermore, the electrode acts also as an interface between the current injecting lead which is an electronic conductor and the body tissue or the electrode gel, which are ionic conductors. Therefore, when a metallic electrode contacts with an electrolyte, ionic conductor, an ion–electron exchange occurs as a result of an electrochemical reaction. Due to this ion-electron exchange, a double layer of charges exists at the interface, and such a system behaves like a parallel plate capacitor.

Thus the interface impedance, also known as skin-electrode interface, can be represented by several equivalent circuit models with more or less detail; see Fig.2.14.

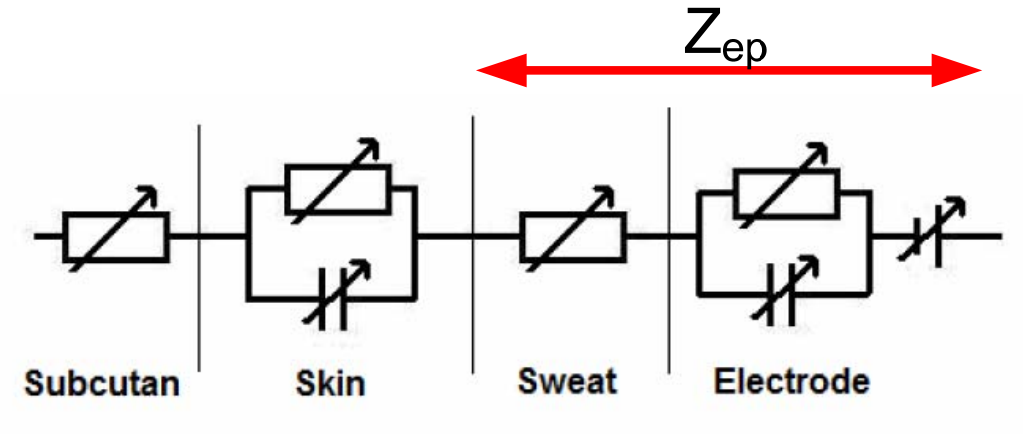

Fig.2.14. Equivalent circuit describing the electrical behaviour of skin-electrode contact.

This impedance, $\mathbf{Z_{ep}}$, is built up by the sweat and the electrode it-self and its value is typically unknown and frequency and time dependent.

2.3.2. EBI Measurement Configurations

2.3.2.1. Two-Electrode Measurement

In this configuration, the injecting leads and the signal sensing leads are connected to the same pair of electrodes. The known excitation signal is applied on the load by using a pair of electrodes, and the resulting response is sensed by the same electrodes; see Fig.2.15.

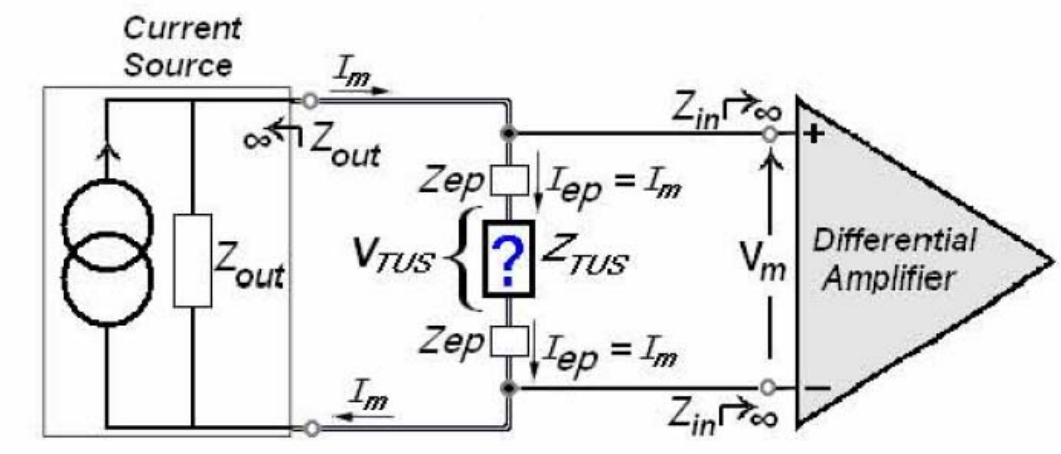

Fig.2.15. Typical 2-wire configuration.

As observed, there is an important inconvenient for the two-electrode configuration. Using the same electrode to excite and to measure, the skin-electrode impedance, $\mathbf{Z_{ep}}$, which is in

series with the measuring load, $\mathbf{Z_{TUS}}$, is included in the measurement and it is not possible to differentiated between them, Equation (2.15).

$$Z_m = \frac{V_m}{I_m} \qquad \textbf{Equation (2.12)}$$

$$V_m = V_{ep} + V_{TUS} + V_{ep} = V_{TUS} + 2V_{ep} \qquad \textbf{Equation (2.13)}$$

$$V_{ep} = I_m \cdot Z_{ep} \qquad \textbf{Equation (2.14)}$$

$$Z_m = \frac{V_{TUS} + 2V_{ep}}{I_m} = Z_{TUS} + 2Z_{ep} \neq Z_{TUS} \qquad \textbf{Equation (2.15)}$$

2.3.2.2. Four-Electrode Measurement

In this configuration, the excitation and sensing leads are connected to a two different pair of electrodes. The excitation signal is applied on the load through two points and the resulting signal is sensed at other two points where the impedance is measured. Due to the voltage on the injecting electrodes is not contained in the sensed voltage, the influence of the skin-electrode impedance can be minimized; see Fig.2.16.

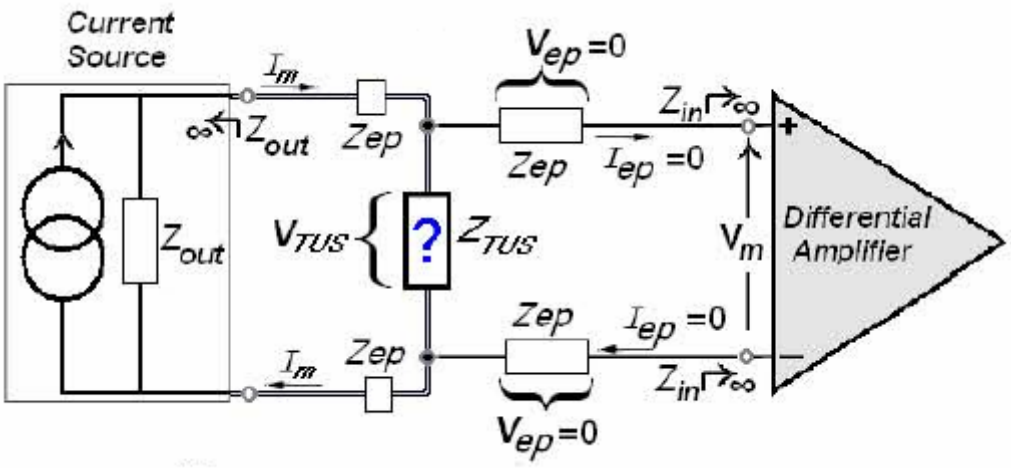

Fig.2.16. Typical 4-wire configuration.

Using Equation (2.12) and Equation (2.13), and since the current through the sensing electrodes is 0, it can be observed as the effect of the electrodes is eliminated in the EBI measurement of the tissue.

$$Z_m = \frac{V_{TUS} + 2V_{ep}}{I_m} = \{V_{ep} \approx 0\} = Z_{TUS} \qquad \textbf{Equation (2.16)}$$

2.4. Wearable Medical Devices [13]

2.4.1. Introduction to Wearable Medical Devices

Nowadays the situation in many national health systems can be described as:

- The life expectancy increases.
- More chronic diseases are appearing, which need to be addressed as early as possible, in order to ensure optimal treatment, even cost-wise.
- Medical advice is asked more often due to people become more health-conscious, but people do not want to spend more times at practices and hospitals.
- The overall cost is ever increasing.

Because of all these issues, laboratory/hospital equipment are not enough and other kind of devices are needed. Wearable Medical Devices (WMDs) can offer a health and patient management system that support continuous monitoring, ubiquitous medical treatment and advice to patients at minimal cost. The idea behind WMDs is to make patients independent of their family doctor, to give them the opportunity to conduct simple measurements on their own and to actively participate in their health care.

2.4.2. Design Requirements & Challenges of WMDs

As "Wearable" (and not only portable) means that the devices are so small and unobtrusive that they accompany the user to any place and any time, and due to achieve the previously mentioned idea, WMDs need to fulfill some design requeriments:

- *Small & Lightweight*: Packaging overhead needs to be minimized due to volume/weight restrictions. Moreover, the WMD shall be unobtrusive in order to be worn as a daily accessory and should not look like a medical device.
- *Low power*: A stand-alone power supply of minimum 15 hrs (= 1 working day) without recharging is mandatory. Apart from low-power components, also the duty cycle shall be used to optimize the power consumption of continuously operated equipment.
- *Housing*: The device shall be shockproof, at least IP65, and biocompatible where exposed to the user. IP65 means according to International Protection Rating (IP), the device shows a complete protection against contact, even no ingress of dust, (range 6) and also shows a water protection against low pressure jets coming from any direction (range 5).
- *I/O interconnection*: If a plug/socket option is selected, this adds mechanical issues and large, expensive hardware. On the other hand, if a wireless connection is selected, much larger power budget is required.
- *Sensors*: Novel sensor concepts are required to be easily integrated into standard electronics or housings.

3.1. System Design Hardware

3.1.1. Introduction

As previously mentioned, the main aim of this project is to design and implement a battery driven measurement system that will be the core of a future wearable bioimpedance device.

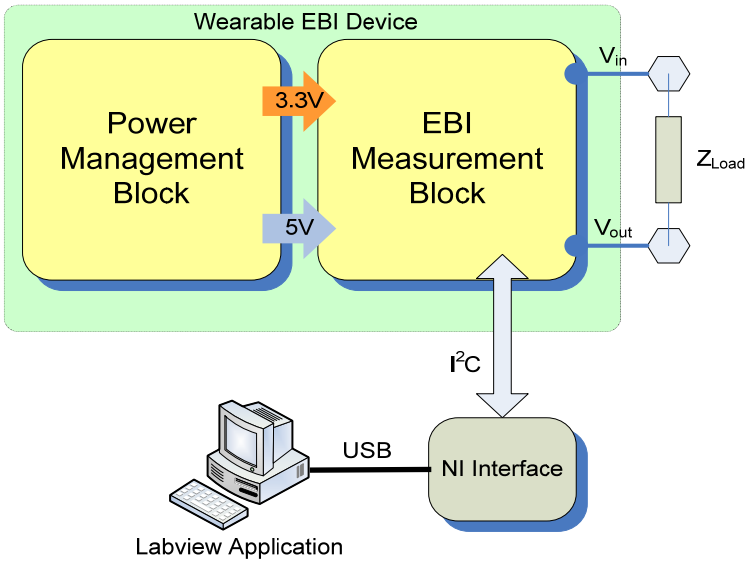

Fig.3.1. Block Diagram of the designed and implemented system.

As Fig.3.1. shows, this wearable bioimpedance device is formed by two main functional modules: the Power Management Block (PMB) and the EBI Measurement Block (EMB). The main task of PMB is to supply the operational voltages, 3.3V and 5V, in order to get the EMB works. The core of the EMB is an Integrated Circuit (IC) manufactured by Analog Devices called AD5933. This IC is a 12-bit precision impedance converter which combines an on-board frequency generator with a 1 MSPS analog-to-digital converter (ADC) and a Digital Signal Processor (DSP) engine which performs the impedance estimation. Moreover, a serial I2C port is included as communication interface.

3.1.2. Power Management Block

3.1.2.1. Introduction

As previously mentioned, the aim of this block is to supply the voltage needed to get the system operational. As Fig.3.2. shows, this block is mainly composed by three ICs and some

basic electronic components such as resistances, capacitors or inductors. Using the Smart Power Selector from Maxim-IC, MAX8677A, the source to supply the system with power is selected. In this design, this supply can be provided by an AC Adapter or by a 1 cell Li-Po battery. Due to the System Supply Output (**SYS**) voltage varies depending on the input source, a Step-Up DC-DC Converter, MAX1763, is needed. Thus, a constant value of 5 DC-voltage is supplied to the rest of the system. Furthermore, using a Linear Regulator, LM1117, a 3.3 DC-voltage is also supplied.

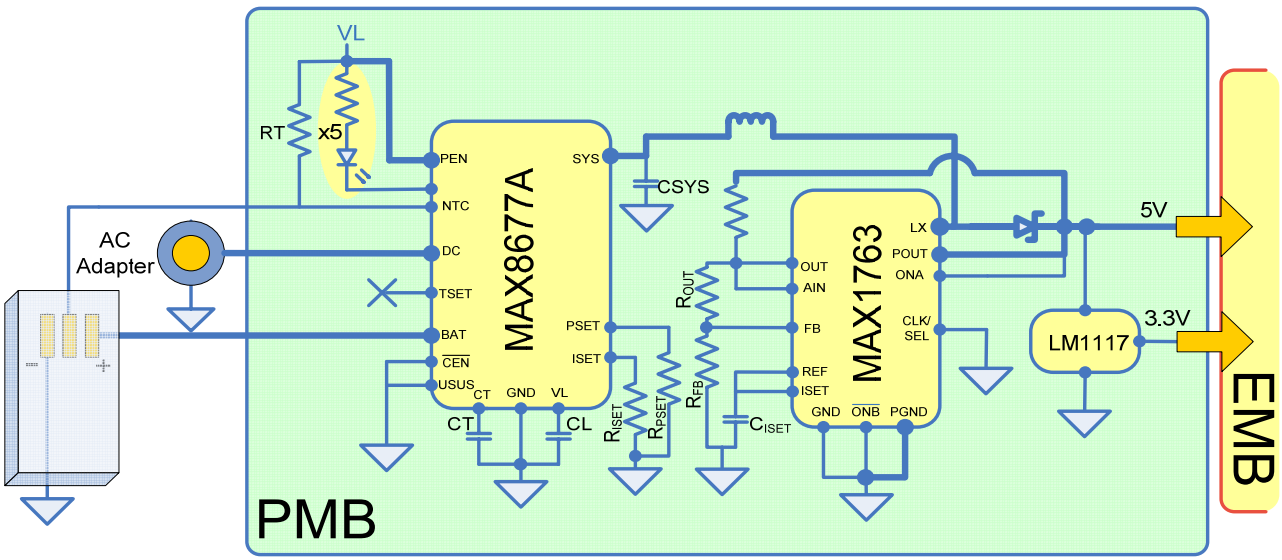

Fig.3.2. Power Management Scheme where all the components except of some capacitors are showed.

3.1.2.2. MAX8677

The MAX8677A is available in a 4mm x 4mm, in a 24-pin TQFN-EP package. It works as an integrated 1-cell Li+ charger and Smart Power Selector™ with dual (DC and USB) power inputs. Furthermore, its main features are:

- ❖ Complete Charger and Smart Power Selector.
- ❖ External MOSFETs are not required because of all power switches for charging and switching the load between battery and external power are included on-chip.
- ❖ Can operate with either separate inputs for USB and AC adapter power, or from a single input that accepts both.
- ❖ System operates with discharged or no battery.
- ❖ Automatic input selection switches the system load from battery to external power.
- ❖ Includes an input Overvoltage Protection (OVP) to 16V.
- ❖ 40mΩ System-to-Battery Switch.
- ❖ On-chip thermal regulation prevents overheating.
- ❖ Includes some indicators such as charge status and fault outputs, power-OK monitors, charge timer, and battery thermistor monitor.

The Table 3-I shows the chief electrical characteristics extracted from its datasheet:

TABLE 3-I: MAX8677A ELECTRICAL SPECIFICATIONS.

PARAMETER		MIN	TYP	MAX	UNITS
DC-TO-SYS PREREGULATOR					
DC Operating Range		4.1		6.6	V
DC Undervoltage Threshold		3.95	4.0	4.05	V
DC Overvoltage Threshold		6.8	6.9	7.0	V
DC Supply Current			1	2	mA
DC-to-BAT Dropout Voltage		10	50	90	mV
DC Current Limit (R_{PSET} = 1.5kΩ)		1800	2000	2200	mA
PSET Resistance Range		1.5		6.3	kΩ
SYS Regulation Voltage		5.1	5.3	5.5	V
VL Voltage		3.0	3.3	3.6	V
CHARGER					
BAT-to-SYS On-Resistance			0.04	0.08	Ω
BAT Regulation Voltage		4.158	4.2	4.242	V
BAT Charge-Current Set Range		0.3		1.5	A
ISET Voltage		0.9	1.0	1.1	V
BAT Prequal Threshold		2.9	3	3.1	V
BAT Leakage Current			3	6	µA
DONE Threshold as a Percentage of Fast-Charge (VTSET = open)			10		%
Maximum Prequal Time			30		Min
Maximum Fast-Charge Time			300		Min
LOGIC I/O: CHG, FLT, DONE, DOK, UOK, PEN1, PEN2, CEN, TSET, USUS					
Logic Input Thresholds	High Level	1.3			V
	Low Level			0.4	
	Hysteresis		50		mV
TSET Input Threshold	High Level	VL – 0.3			V
	Midlevel	1.2		VL-1.2	
	Low level			0.3	
Logic Input-Leakage Current			0.001	1	µA

***USB specifications are not showed because of USB input is not used in this system.**

Paying attention to its blocks diagram, Fig.3.3., it can be observed the MAX8677A contains a Li-Po charger, as well as power MOSFETs and control circuitry to manage power flow. The Smart Power Selector circuitry offers flexible power distribution from an AC adapter or USB source to the battery (**BAT**) and system load (**SYS**). In our specific design, as the USB source input is cancelled, only the AC adapter source input (**DC**) supplies power. Therefore, if both an external power supply and battery are connected, the battery is charged with residual power from the DC input when the system load requirements are less than the input current limit. On the other hand, if both are connected but the system load requirements exceed the input current limit, the battery supplies supplemental current to the load. Finally, if there is no external supply connected, the system is powered from the battery.

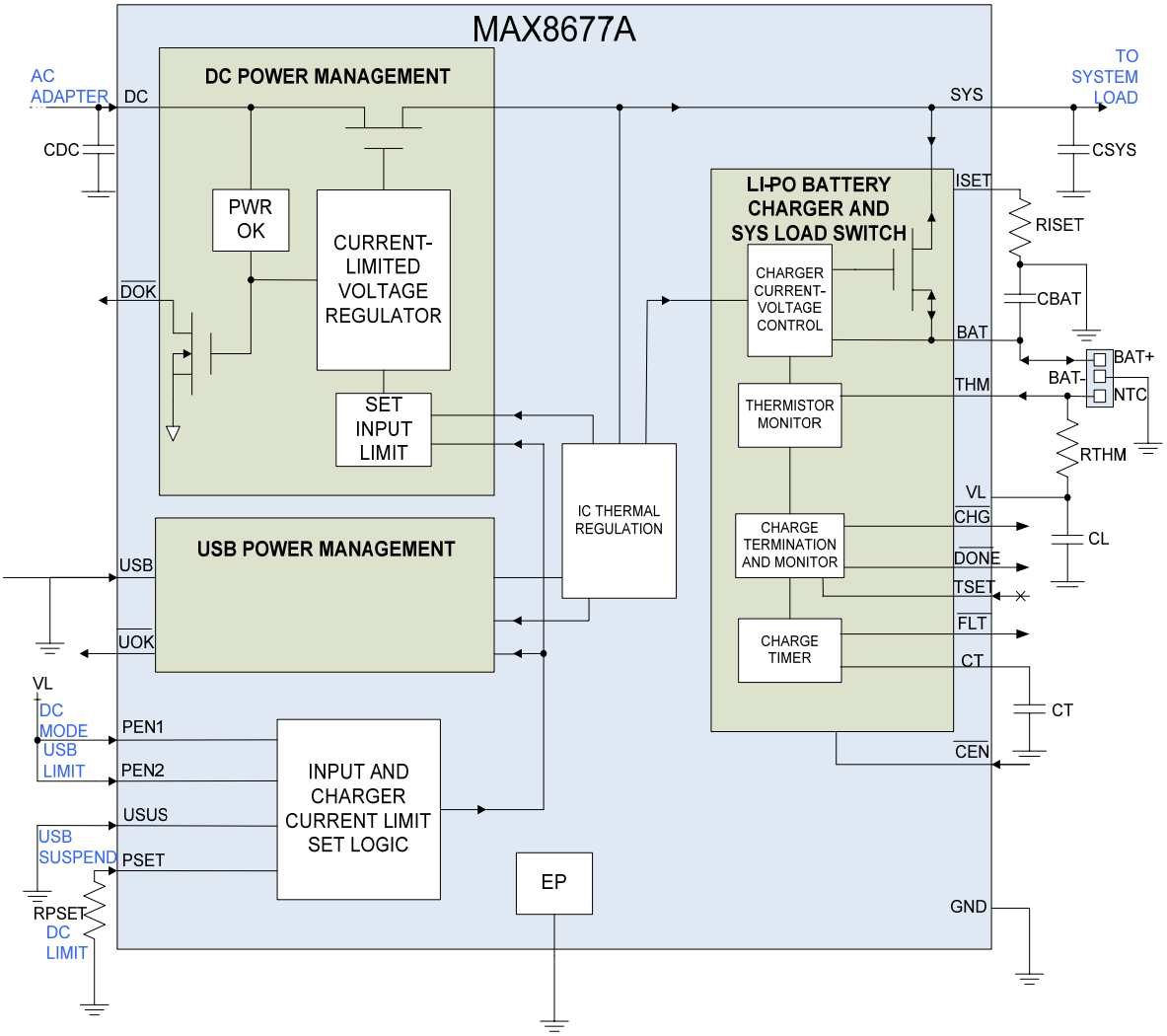

Fig.3.3. MAX8677A Block Diagram. Due to the USB Power Management block is like DC Power Management block, this is not showed in detail.

The Input & Charger Current Limit Set Logic block controls the total SYS current, which is the sum of the system load current and the battery-charging current, through the logic inputs PEN1, PEN2 and USUS, and the analog inputs PSET and ISET; see Table 3-II.

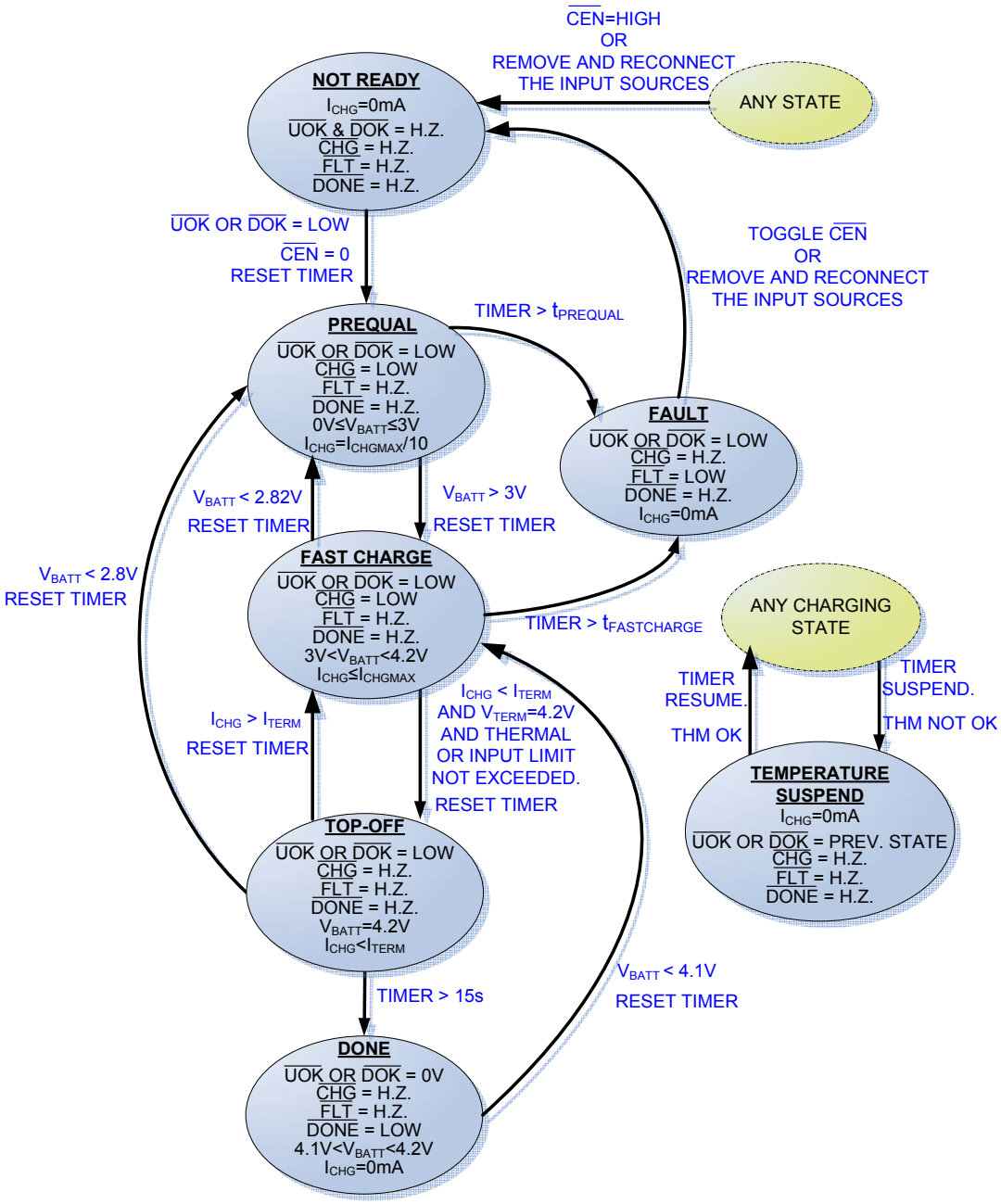

Fig.3.4. MAX8677A Charger State Flowchart where H.Z. means High Impedance.

TABLE 3-II: INPUT LIMITER CONTROL LOGIC.

POWER SOURCE	DOK	UOK	PEN1	PEN2	USUS	DC INPUT CURRENT LIMIT	MAXIMUM CHARGE CURRENT
AC Adapter at DC Input	L	X	H	X	X	$3000/R_{PSET}$	$3000/R_{ISET}$
DC and USB unconnected	H	H	X	X	X	No DC input	0

As in this design, the USB input is cancelled, the logic inputs PEN2 and USUS, which set the USB current limit, are not important. As PEN1 is always high, connected to VL, the DC input current limit is set by the value of R_{PSET}. Thus, as R_{PSET} is a fixed value of 1.5kΩ, a 2A DC input current limit is also set. Furthermore, ISET adjusts the maximum fast-charge current to match the capacity of the battery through a resistor, R_{ISET}. In this design a 1A value of maximum charge current is set by a value of 3kΩ of R_{ISET}.
The battery charger initiates a charge cycle when the charger is enabled and there is a valid DC or USB input. See the charging state diagram illustrated in Fig.3.4. Firstly it detects the battery voltage and if it is less than the BAT prequal threshold (3.0V) then the charger enters into prequal mode, in which the battery charges at 10% of the maximum fast-charge current. This reduced charge rate ensures that the battery is not damaged by the fast-charge current while deeply discharged. Once the battery voltage rises to 3.0V, the charger transitions to fast-charge mode and applies the maximum charge current. Finally the battery voltage rises until it approaches the battery regulation voltage (4.2V). When charge current decreases to the value of fast-charge current set by TSET, 10% in this design, the charger enters a brief 15s top-off, and then charging stops. If the battery voltage subsequently drops below the 4.1V recharge threshold, charging restarts and the timers reset.

3.1.2.3. MAX1763

The MAX1763 is a high-efficiency, low-noise, step-up DC-DC converter proposed to use in battery-powered applications which require the longest possible battery life. Its main features are:

- ❖ High Efficiency, usually up to 94%.
- ❖ It is possible to generate a fixed 3.3V Output or an Adjustable (2.5V to 5.5V) one from a wide range of input voltage (+0.7V to +5.5V).
- ❖ Guarantees startup with an input voltage as low as 1.1V.
- ❖ The output voltage is generated by a 1MHz synchronous-rectified PWM boost topology with up to 1.5A output capability.
- ❖ Includes an on-chip linear gain block to build an external linear regulator or a low-battery comparator.
- ❖ Also includes a 1μA logic-controlled shutdown block and some soft-start and current limit functions to optimize the system.

Table 3-III shows some main electrical characteristics extracted from the MAX1763's datasheet:

TABLE 3-III: MAX1763 ELECTRICAL SPECIFICATIONS.

PARAMETER		MIN	TYP	MAX	UNITS
DC-DC SWITCHES					
POUT Leakage Current			0.1	10	µA
LX Leakage Current			0.1	10	µA
N-Channel Current Limit		2.0	2.5	3.4	A
P-Channel Current Limit		10	120	240	mA
REFERENCE					
Reference Output Voltage		1.230	1.250	1.270	V
Reference Supply Rejection			0.2	5	mV
GAIN BLOCK					
AIN Reference Voltage		910	938	970	mV
Transconductance		5	10	16	mS
Gain Block Enable Threshold (V_{OUT}-V_{AIN})				1.4	V
Gain Block Disable Threshold (V_{OUT}-V_{AIN})		0.2			V
DC CONVERTER					
Input Voltage Range			0.7	5.5	V
Minimum Startup Voltage			0.9	1.1	V
Output Voltage		3.17	3.3	3.38	V
FB Regulation Voltage		1.215	1.245	1.270	V
FB Input Current (V_{FB} = 1.35V)			0.01	100	nA
Output Voltage Adjust Range		2.5		5.5	V
Output Voltage Lockout Threshold		2.00	2.15	2.30	V
ISET Input Leakage Current			0.01	50	nA
No-Load Supply Current, Low-Power Mode			110	200	µA
LOGIC INPUTS					
CLK/SEL Input	High Level	(0.8) V_{OUT}			V
	Low Level			(0.2) V_{OUT}	
ONA and ONB Input	High Level	1.6			V
	Low Level			0.4	
Minimum CLK/SEL Pulse Width			100		ns
Maximum CLK/SEL Rise/Fall Time			100		ns
Logic Input-Leakage Current			0.01	1	µA

Although MAX1763 has 3 Operating Modes depending on the source connected to

CLK/SEL input (logic 0, logic 1 or external clock), in this design only the Normal Operation can be selected (CLK/SEL = LOW); See Fig.3.5.

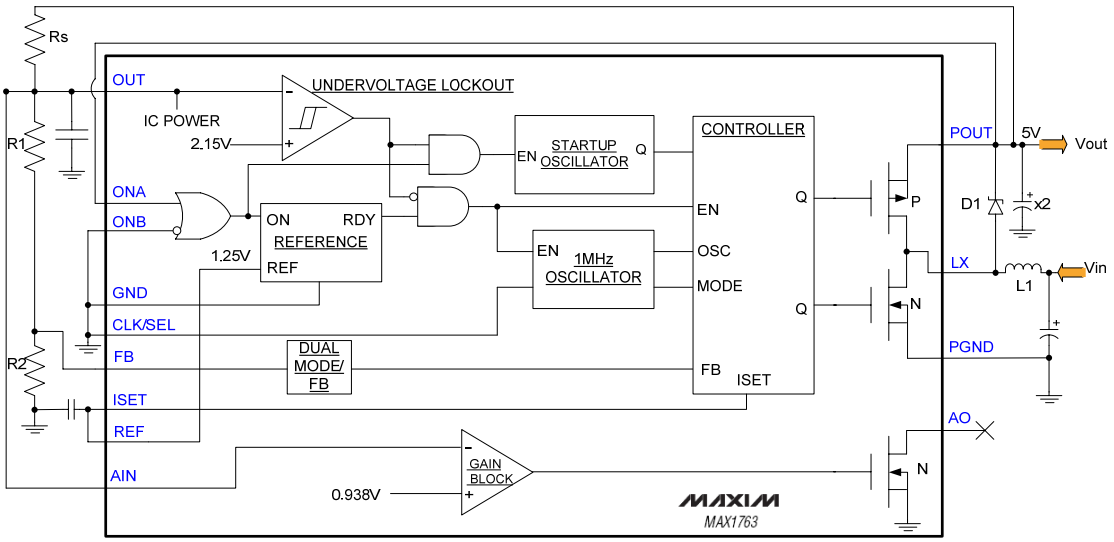

Fig.3.5. MAX1763 Block Diagram using the Normal-Mode Operation and setting the Output Voltage at 5V.

During DC-DC converter operation, the internal N-channel MOSFET switch turns on for the first part of each cycle, allowing current to ramp up in the inductor (L1) and store energy in a magnetic field. During the second part of each cycle, the MOSFET turns off and inductor current flows through the synchronous rectifier to the output filter capacitor and the load. As the energy stored in the inductor is depleted, the current ramps down and the synchronous rectifier turns off, the N-channel FET turns on and the cycle repeats. With small loads, depending on the operating mode, the output voltage is regulated using either PWM or by switching only as needed to service the load. In its normal mode of operation, the MAX1763 operates in PWM when driving medium to high loads and at light loads it only switches as needed. This optimizes efficiency over the widest range of load conditions. It offers fixed-frequency PWM operation through most of its load range. Furthermore, in this design, an external Schottky diode (D1) must be connected from LX to POUT pin because the output voltage is greater than 4V (V_{POUT} = 5V). To reach this output voltage value, a resistor voltage-divider to FB from OUT to GND is needed. Thus, accordingly with the device's datasheet (Equation (3.1)), the values of R1 and R2 are chosen:

$$R_1 = R_2\left(\frac{V_{OUT}}{V_{FB}} - 1\right) \xrightarrow{\left\{\begin{array}{l} V_{OUT}=5 \\ V_{FB}=1.245V \\ R_2 \le 30k\Omega \end{array}\right\}} \begin{array}{l} R_1 = 82k\Omega \\ R_2 = 27k\Omega \end{array} \qquad \textbf{Equation (3.1)}$$

3.1.3. EBI Block

3.1.3.1. Introduction

As previously mentioned and it is also showed in Fig.3.6, the core of this block is the IC called AD5933.

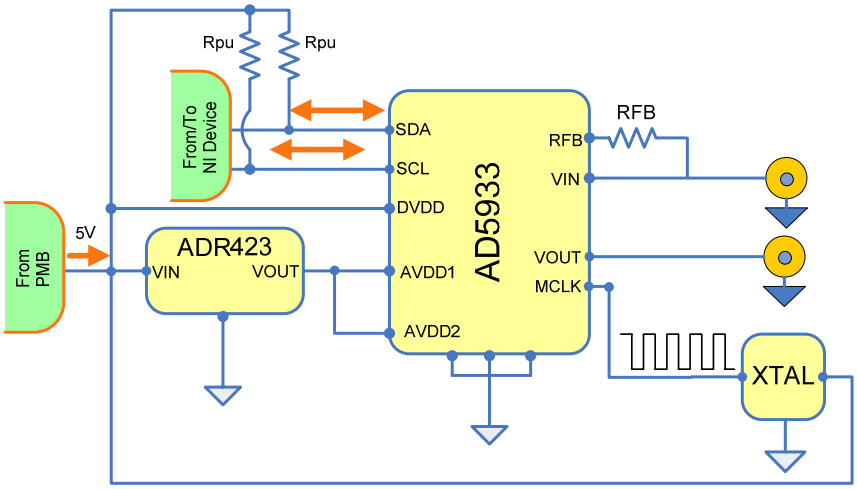

Fig.3.6. EBI Block without any capacitors.

As showed, 5V are supplied by the Power Management Block. Furthermore, the I2C module is connected to a National Instrument (NI) Device to configure the AD5933. Thus, the IC estimates the load between V_{in} and V_{out} pins and the result is sent by the I2C module to a Labview application though the NI Device.

3.1.3.2. AD5933

This IC is a high precision impedance converter system composed by several blocks, as illustrated Fig.3.7. In the *exciting channel*, sine waveforms are generated digitally by a 27-bit Direct Digital Synthesizer (DDS); see Fig.3.8 to know as the DDS works. The clock of this DDS is generated by either an external clock which is connected to the MCLK pin or by an internal clock. Thus, once the analog waveform is generated, it is amplified through a programmable gain stage and a programmable voltage output excitation is set up. Although there are four different ranges, in this design it is only used Range 1. In this range, the output excitation voltage amplitude and the output DC Bias level are, respectively, 1.98 V_{p-p} and 1.48 V.

Later, this output excitation signal at a particular frequency is applied to the measuring load, which is connected between V_{OUT} and V_{IN} pins. Therefore, as a response to this excitation voltage, a current is flowing through the working impedance and it is acquired by the *Response channel*. This stage is a current sensing stage and it is composed by a current-to-voltage amplifier followed by a programmable gain amplifier (PGA), an antialiasing filter, and an ADC. Thus, the current flowing through the unknown impedance becomes a voltage signal at the output of the current-to-voltage converter. The gain of this current-to-voltage

amplifier is chosen by the user connecting a feedback resistance between RFB and VIN pins. It is very important to maintain the signal within the linear range of the ADC (0V to VDD). To get this, both the feedback resistance and the PGA gain must be calculated following the Equation (3.2).

$$Gain = Output\ Excitation\ Voltage \times \frac{Gain\ Setting\ resistor}{Zunknown} \times PGA\ Gain \quad \textbf{Equation (3.2)}$$

Finally, the digital data from the ADC is passed to the DSP core and the DFT is performed. The DFT algorithm used in AD5933 consists on a multiplication which is accumulated over 1024 samples for each frequency point; see Equation (3.3). The result of this DFT is stored in twos complement format in two, 16-bit registers: the real and the imaginary registers.

$$X(f) = \sum_{n=0}^{1023} \left(x(n) \left(\cos(n) - j \sin(n) \right) \right) \quad \textbf{Equation (3.3)}$$

Where X(f) is the power in the signal at the Frequency Point f, x(n) is the ADC output, cos(n) and sin(n) are the sampled test vectors provided by the DDS core at the Frequency Point f, and j is the imaginary value $\sqrt{-1}$.

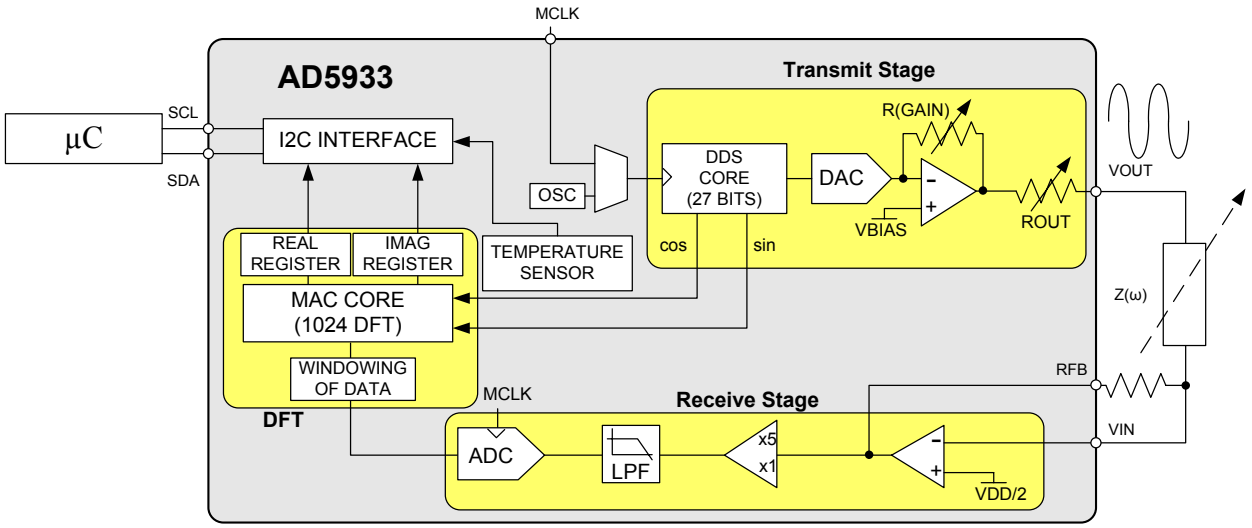

Fig.3.7. AD5933 Functional Block Diagram. There are 3 main blocks: Transmit and Receive Stages and DFT.

As observed, this IC is quite complete and its registers have not been showed yet. In the next section, a Labview software, which configures these registers and uses the stored data, is presented. But before that, some main electrical specifications are shown in the Table 3-IV.

TABLE 3-IV: AD5933 ELECTRICAL SPECIFICATIONS.

PARAMETER		MIN	TYP	MAX	UNITS
SYSTEM					
Impedance Range		1k		10M	Ω
Total System Accuracy			0.5		%
TRANSMIT STAGE					
Output Frequency Range		1		100	kHz
Output Frequency Resolution			0.1		Hz
MCLK Frequency				16.776	MHz
TRANSMIT OUTPUT VOLTAGE (Range 1)					
AC Output Excitation Voltage			1.98		Vp-p
DC Bias			1.48		V
DC Output Impedance			200		Ω
RECEIVE STAGE					
Input Leakage Current			1		nA
Input Capacitance			0.01		pF
Feedback Capacitance			3		pF
ANALOG-TO-DIGITAL CONVERTER					
Resolution			12		Bits
Sampling Rate			250		kSPS
POWER REQUIREMENTS					
VDD		2.7		5.5	V
IDD	Normal mode		10	15	mA
	Standby mode		11		
	Power-Down mode		0.7	5	µA
LOGIC INPUTS					
Input Voltage	High Level	0.7 x VDD			V
	Low Level			0.3 x VDD	

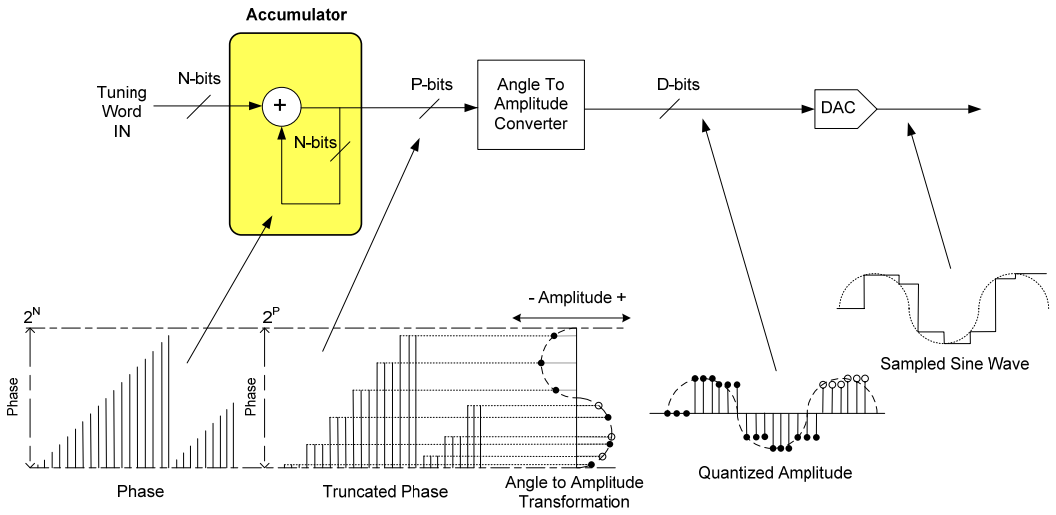

Fig.3.8. DDS Block Diagram. The Sampled Sine Wave is obtained through an angle to amplitude converter which transforms the truncated phase into an amplitude value. [14]

3.1.4. Implementation Board

This wearable EBI device has been designed using a software called OrCAD. It is a proprietary software tool suite used primarily for electronic design automation. Therefore, it is used mainly to create electronic prints for manufacturing of printed circuit boards. Furthermore, this software also allows to create electronic schematics and diagrams being able to simulate them.
Once the PCB has been design through the OrCAD Layout Application, the final board has been manufactured out of the university by an external company. The main reason to do this has been because of almost all components have been chosen in SMD packages to reduce the size and the weight of the final board as soon as possible. Thus, the final board is showed in Fig.3.9. and it can be observed as all components have been placed on the top and the battery on the bottom.

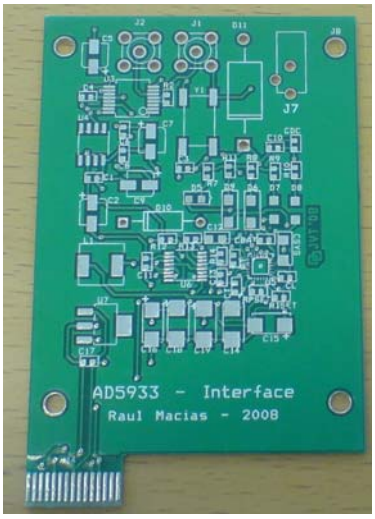

Fig.3.9. Final Board Top Layer.

3.2. Software Implementation

3.2.1. Introduction

As previously mentioned, the AD5933 has an I2C interface. Through this, AD5933 is configured with the desired parameters to estimate the impedance and later, this result can be sent by the I2C interface to other application to be processed or evaluated. As it will be explained in the next sub-section, the I2C protocol is a Master-Slave communication. In our design, the AD5933 acts as a Slave and as a Master, the NI I2C/SPI Interface called USB-8451 has been chosen.

This device allows to connect to and to communicate with I2C, SMBus, and SPI devices. Furthermore, it is a good solution to communicate with consumer electronics such as PCs or Laptops due to its plug-and-play USB connection. Thus, using this device, the implemented board is connected to a PC where runs a Labview application.

Fig.3.10. NI USB-8451 device.

3.2.2. I2C Protocol [15] [16] [17]

3.2.2.1. I2C Introduction

I2C is a multi-master serial computer bus invented by Philips and it is used to attach low-speed peripherals to a motherboard or an embedded system.
I2C has only two bi-directional lines called Serial Data (SDA) and Serial Clock (SCL) to carry information between the devices. Due to the fact that there is only a unique line for data, the I2C is a half-duplex system; a device cannot receive and send data at the same time.
Each device is usually recognized by a unique 7-bit address, although a 10-bit address is also possible. Furthermore, I2C devices can operate as Master or Slave. The main tasks of a Master device are to generate and control the clock signal, to start and stop the data transfer process and to control addressing of other devices. The Slave device is the one that is addressed by the Master. Furthermore, both of them, Master and Slave, act as Transmitter and Receiver in two common mode of operation: a Master-transmitter sends data to a Slave-receiver or a Master-receiver requires data from a Slave-transmitter.

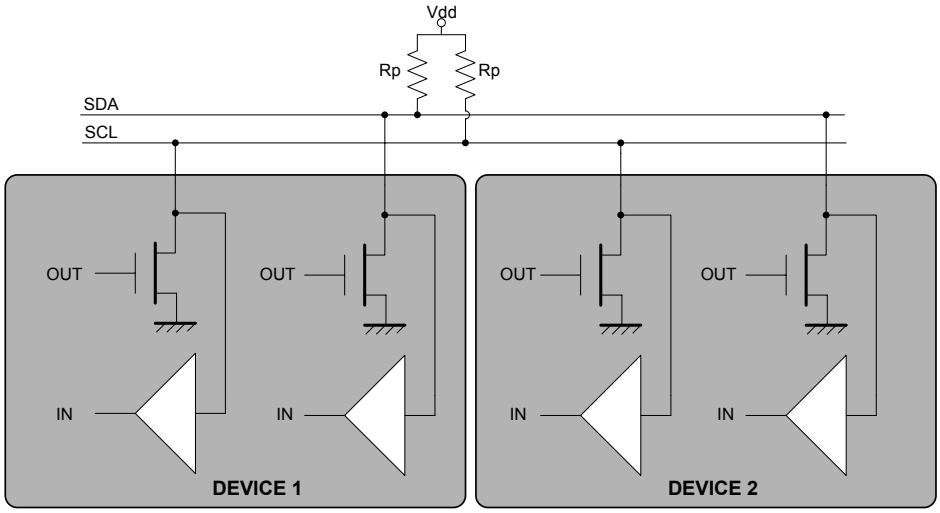

Fig.3.11. Typical I2C connection. The device outputs are wired with signal on bus.

Depending on the speed which the data are transferred, there are three modes: Standard Mode (100kbps), Fast Mode (400kbps) and High Speed Mode (3.4Mbps).
About the maximum number of devices which can be connected together, it is limited by the address space and also by the total bus capacitance of 400 pF.

3.2.2.2. I2C Bus Characteristics

Depending on the state of both SDA and SCL lines, during a communication the following scenarios can occur:

- Idle State: This situation happens when the I2C bus is not busy and both lines remain high due to the pull-up resistors. It can be observed that after a Stop Condition (P) and before next Start Condition (S).

- ❖ Start Condition (S): This situation occurs during a High to Low transition of SDA line while the SCL remains high.
- ❖ Stop Condition (P): It is a Low to High Transition of SDA line while SCL remains high.
- ❖ Data Valid: Data are valid when the SCL is high. Data must be stable during high clocks and it can change only during low clocks. Every data bit is only interpreted per one clock pulse. If any change occurs in SDA while SCL is high, it will be interpreted as S or P condition.
- ❖ Acknowledge (ACK): Each device generates an ACK signal after the reception of each byte. The master generates an extra clock pulse and if the device pulls down the SDA line, an ACK is interpreted. On the other hand, if SDA is high, a Not-ACK (NACK) is interpreted.

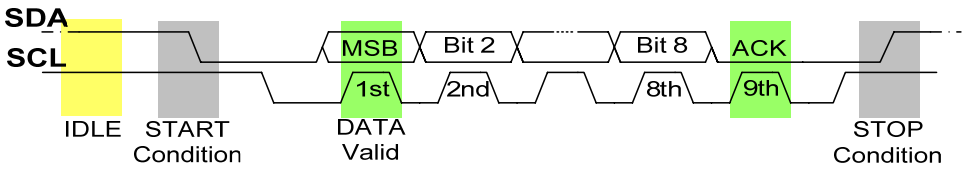

Fig.3.12. Timing Diagram.

3.2.2.3. I2C Protocol

I2C follows a master/slave protocol. The master is the device which always initiates the communication. For it, the master sends a start condition which informs all the slave devices to listen for instructions on the SDA. After that, the master sends the 7-bit address of the target slave and a read/write flag (low logic level to write to the slave and high logic level to read from the slave). If the slave with the matching address exists, it responds with an ACK. Thus, the communication proceeds between the master and the slave on SDA. Both the master and slave can receive or transmit data depending of the flag value. The transmitter sends 8-bits of data to the receiver which replies with a 1-bit acknowledgement when it receives the byte. Finally, when the communication is complete, the master sends a stop condition indicating that everything is done.

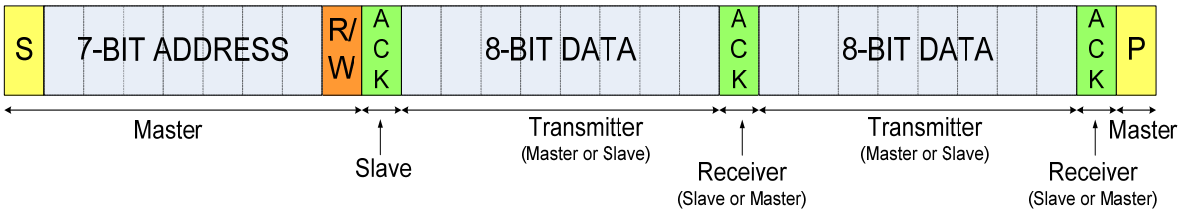

Fig.3.13. I2C generic Protocol. First, Master sends start (S), slave address and R/W flag and Slave answers an ACK. Later, Transmitter is sending 1-byte data and Receiver is answering with an ACK. Finally, Master sends a Stop Condition (P) to indicate the communication is over.

3.2.3. Labview Application

3.2.3.1. Introduction

Our designed board is connected to a PC running a Labview application by the NI I2C/SPI Interface. Labview is a platform and development environment for a visual programming language, called "G", created by National Instruments. It is used by scientists and engineers for several tasks such as data acquisition, automated test and instrument control, industrial measurements and control, and embedded design.

As Labview is a visual programming language, there is no need to write any code. A Labview program consists of a several linked blocks known as Virtual Instruments, VIs. Through the designed application, it is allowed to configure the AD5933 and to process the data stored in real and imaginary registers. In the next sub-sections, all of the Vis designed in this project are showed and explained.

3.2.3.2. AD5933 Configuration Blocks

The AD5933 permits the user to perform some features before estimation is made. To configure these user-defined parameters, a new VI, called FreqMeas, has been created. This VI has seven inputs and four outputs; see Fig.3.14.

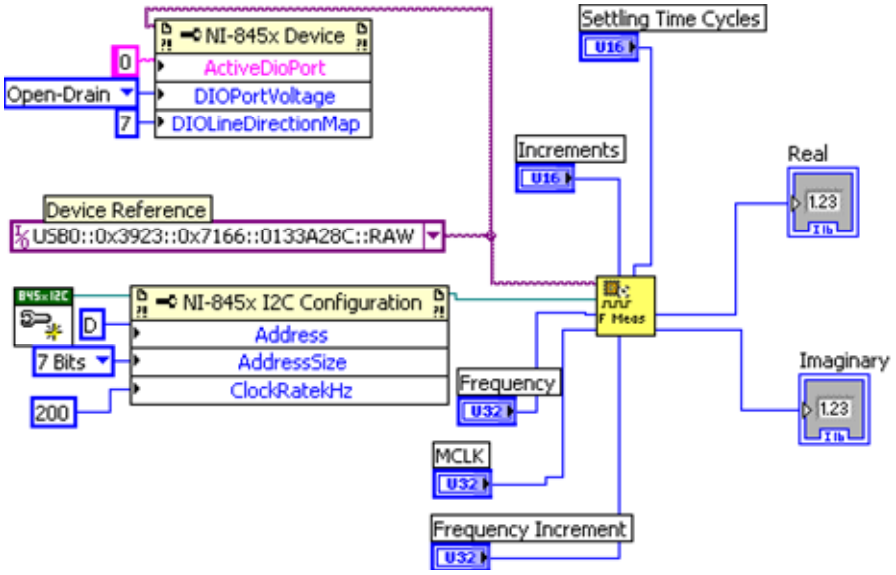

Fig.3.14. FreqMeas VI. Its 7 inputs and only 2 outputs are showed.

Through this VI, the user can define the start frequency (*Frequency*), the frequency resolution (*Frequency Increment*), and number of points in the frequency sweep (*Increments*). Furthermore, the value of the clock (*MCLK*) and the number of settling time cycles (*Setting Time Cyles*), which determines the number of output excitation cycles can pass through the unknown impedance before ADC conversion starts, must be added. The other two inputs are used to indicate that the NI-845 is the master device and to configure the speed and addressing, 7-bit address in this case, in the I2C protocol. Moreover, AD5933 address is also indicated as 0x0D in hexadecimal or 0b0001101. As noticed, only 7 bits are

used to indicate the slave address due to 8th bit, LSB, is used as a Read or Write flag and it is the NI-845 software which internally sets this bit to the correct value.
Finally, the outputs called *Real* and *Imaginary* show the value which is stored in these registers.
Before explaining this VI in more detail, the Table 3-V shows the AD5933 Register Map.

TABLE 3-V: AD5933 REGISTER MAP.

Name		Register
Control	High (D15 to D8)	**0x80**
	Low (D7 to D0)	**0x81**
Start Frequency	High (D23 to D16)	**0x82**
	Middle (D15 to D8)	**0x83**
	Low (D7 to D0)	**0x84**
Frequency Increment	High (D23 to D16)	**0x85**
	Middle (D15 to D8)	**0x86**
	Low (D7 to D0)	**0x87**
Number of Increments	High (D15 to D8)	**0x88**
	Low (D7 to D0)	**0x89**
Number of Settling Time Cycles	High (D15 to D8)	**0x8A**
	Low (D7 to D0)	**0x8B**
Status	D7 to D0	**0x8F**
Real Data	High (D15 to D8)	**0x94**
	Low (D7 to D0)	**0x95**
Imaginary Data	High (D15 to D8)	**0x96**
	Low (D7 to D0)	**0x97**

To explain in detail this VI, it is easier to show all the steps through a flowchart; see Fig.3.15. The first Stage in the flowchart represents the four frames at the beginning of the VI Sequence. The values of the Start Frequency and the Frequency Increment are calculated following, respectively, the Equation (3.4) and the Equation (3.5).

$$Start\ Frequency\ Code = \left(\frac{\text{Required Output Start Frequency}}{\left(\frac{MCLK}{4} \right)} \right) \times 2^{27} \qquad \textbf{Equation (3.4)}$$

$$Frequency\ Increment\ Code = \left(\frac{\text{Required Frequency Increment}}{\left(\frac{MCLK}{4} \right)} \right) \times 2^{27} \qquad \textbf{Equation (3.5)}$$

Later, these values and the values of the Number of Increments and the Number of Settling Time Cycles are split in 1-byte blocks and stored in their relevant registers. Although the number of settling time cycles can be increased by a factor of 2 or 4 depending upon the status of the bits D10 and D9, in this design this increase factor is not used. Thus, the value stored in the register 0x8A must not be changed.
In the second stage, AD5933 is placed into Standby Mode writing in the High Control Register (0x80) the value 0xB0. Due to Control Register and Status Register are often used, they are shown in the Table 3-VI.

TABLE 3-VI: CONTROL & STATUS REGISTER MAP.

Control Register											
Control Register	High Register	Bit				Function	Bit				Function
		D15	D14	D13	D12		D11	D10	D9	D8	
		0	0	0	1	Initialize with start frequency	x	0	0	x	2.0 Vp-p typical
		0	0	1	0	Start frequency sweep	x	0	1	x	200 mVp-p typical
		0	0	1	1	Increment frequency	x	1	0	x	400 mVp-p typical
		0	1	0	0	Repeat frequency	x	1	1	x	1.0 Vp-p typical
		1	0	0	1	Measure temperature	x	x	x	0	PGA gain x5
		1	0	1	0	Power-down mode	x	x	x	1	PGA gain x1
		1	0	1	1	Standby mode					
	Low Register	Bit				Function	Bit				Function
		D7	D6	D5	D4		D3	D2	D1	D0	
		0	0	0	0	No Reset	0	0	0	0	Internal clock
		0	0	0	1	Reset	1	0	0	0	External clock

Status Register									
Status Register	D7	D6	D5	D4	D3	D2	D1	D0	Function
	0	0	0	0	0	0	0	1	Valid Temperature measurement
	0	0	0	0	0	0	1	0	Valid Real/Imaginary Data
	0	0	0	0	0	1	0	0	Frequency sweep Complete

In the third stage, firstly AD5933 is configured to use the internal system clock, a PGA gain factor of x1 and an excitation voltage of 2.0Vp-p typical (Range 1). Thus, a value of 0x00 and a value of 0x01 are written in the Low and High Control Registers, respectively. Finally, AD5933 is programmed with a Initialize with Start Frequency command (value 0x10 in High Control Register).
In the next stage, after a constant delay has elapsed, a Start Frequency Sweep command (0x20) is write in the High Control Register. Then, after waiting a sufficient amount of time, which has been calculated depending on the number of settling time cycles and the value of the frequency, the Status register is polled to check if the DFT conversion is complete. To check this, a value of 0x02 must be stored in the Status register.

When the DFT is complete, the values of the Real and Imaginary registers are read. Due to both of these values are stored in 16-bit, twos complement format, they must be decoded.
In the final stage, AD5933 is programmed into Power-down mode. This stage is implemented out of the FreqMeas VI.

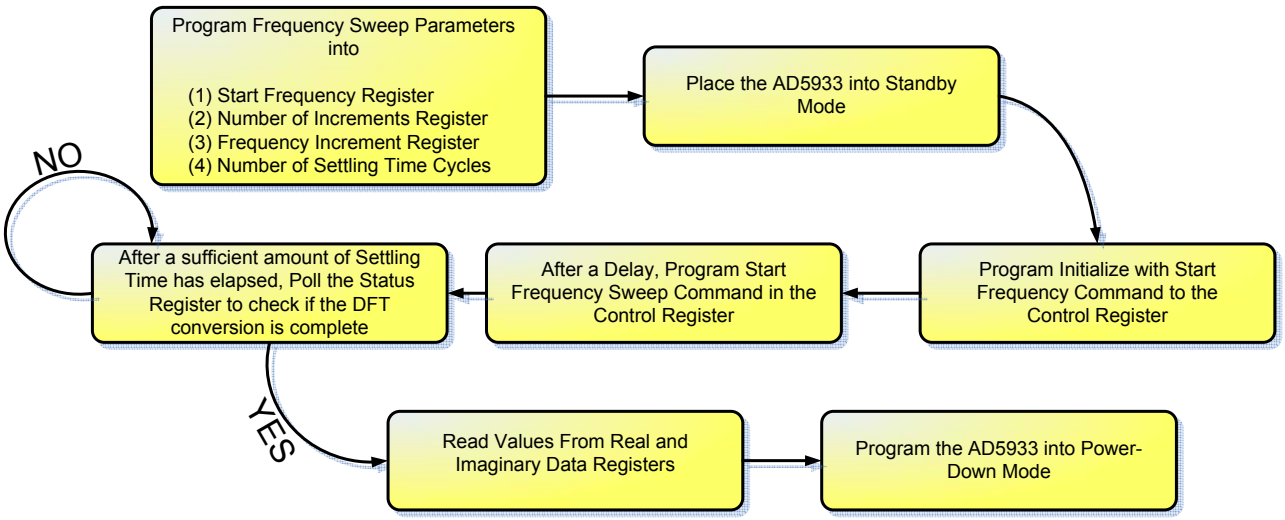

Fig.3.15. AD5933 Frequency Sweep Flowchart.

3.2.3.3. Impedance Magnitude Calculation

After reading values from Real and Imaginary Data registers, the magnitude is calculated by the Equation (3.6).

$$Magnitude = \sqrt{R^2 + I^2} \qquad \textbf{Equation (3.6)}$$

Where R is the real number stored in High and Low Real registers, and I is the imaginary value stored in High and Low Imaginary registers.
But this value is not the real estimated value of the impedance magnitude, to obtain it this value must be multiplied by a gain factor which is calculated during the calibration. To obtain this gain factor, a calibration impedance is connected between VIN and VOUT pins. Thus, after calculating the DFT magnitude at a certain frequency point, the Gain factor is obtained by the Equation (3.7).

$$\text{Gain Factor} = \frac{\left(\frac{1}{\text{calibration Impedance}}\right)}{Magnitude} \qquad \textbf{Equation (3.7)}$$

Due to the fact that the gain factor is frequency-dependent, to minimize the error, in this design the gain factor points are calculated at every single frequency that the impedance will be measured and they are stored in an array. Later, this array is used to compensate the time delay introduced by the circuitry and accurately estimate the true value of the working load impedance. This value is obtained in the same way as the gain factor but using a unknown load instead; see Fig.3.16. Thus, the measured impedance at frequency point is given by the Equation (3.8).

$$\text{Impedance} = \frac{1}{Gain\ \ Factor \times Magnitude} \qquad \textbf{Equation (3.8)}$$

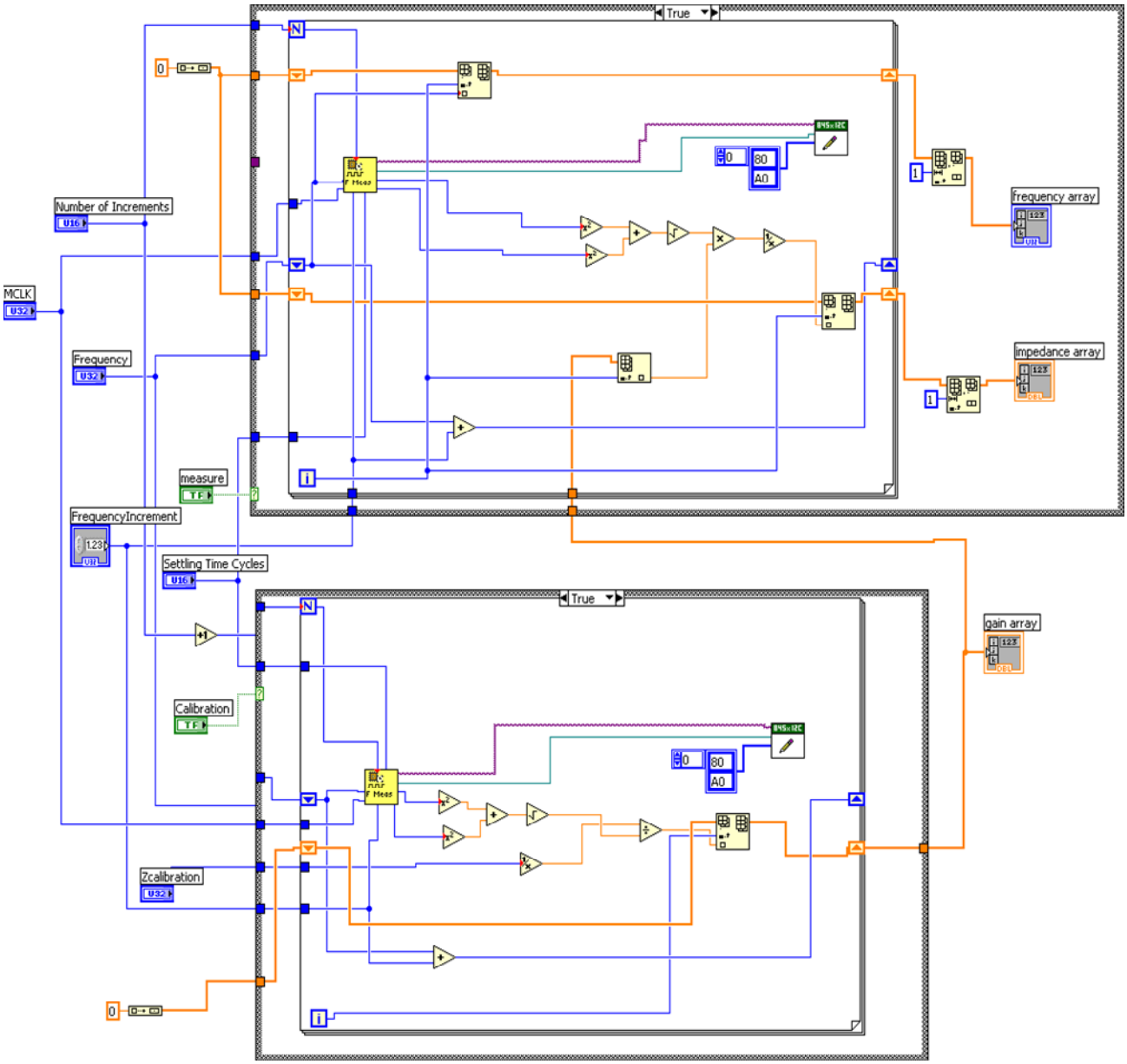

Fig.3.16. AD5933 Calibration and Impedance Magnitude Blocks.

3.2.3.4. Impedance Phase Calculation

As AD5933 stores the real and imaginary values in different registers, the phase across an unknown impedance can be measured according to the Equation (3.9).

$$\text{Phase(rads)} = \tan^{-1}\left(I/R\right) \qquad \textbf{Equation (3.9)}$$

Where $\tan^{-1}$ is the arctangent, I is the imaginary value stored in High and Low Imaginary registers, and R is the real component stored at High and Low Real registers.

As well as in impedance magnitude calculation, a calibration is required due to the AD5933 system phase is added in the measure. Thus, the first step to measure the phase of an unknown impedance consists of measuring the phase, Equation (3.9), placing a resistor between VIN and VOUT pins. Due to the phase of a resistor is zero, the measured phase depends entirely on the AD5933 system.

Once the system phase has been calculated for every certain frequency point and these values have been stored in an array, the phase of an unknown impedance is calculated using the Equation (3.10). Due to the Equation (3.9) is only working on the range between $-\pi/2$ and $\pi/2$ and the correct phase depends on the sign of the real and imaginary component, several conditions are used in the Matlab script, which is used in this application, and are summarized in the Table 3-VII.

TABLE 3-VII: PHASE ANGLE.

Quadrant	Real	Imaginary	Phase Angle (degrees)
1st	+	+	$\tan^{-1}\left(I/R\right)\times\frac{180^0}{\pi}$
2nd	-	+	$180^0+\tan^{-1}\left(I/R\right)\times\frac{180^0}{\pi}$
3rd	-	-	$180^0+\tan^{-1}\left(I/R\right)\times\frac{180^0}{\pi}$
4th	+	-	$360^0+\tan^{-1}\left(I/R\right)\times\frac{180^0}{\pi}$

$$Z\theta = \Phi unknown - \nabla system \qquad \textbf{Equation (3.10)}$$

Where ∇ system is the phase of the system, and Φunknown is the phase of the system and the unknown impedance. Both of these phases are calculated through the Equations summarized in the Table 3-VII. Finally Zθ is the phase due to the unknown impedance.

4.1. Board Electrical Characteristics

4.1.1. Battery Life

To check the battery life time, the system has been tested in two different operation modes. The first one is simulating a Standby mode. No measurements have been taken during the time which the battery voltage has been acquired. The other operation mode is completely the opposite situation, with the system working in Continuous Acquisition mode. In this mode, a sample is measured per second.

Since the operation modes are the opposite of each other the battery time of any other operation mode between these two can be extrapolated. As it is shown in Fig.4.1, the battery life in Standby mode is around 61520 seconds, equivalent to 17 hours 5 minutes and 20 seconds. On the other hand, in the Continuous Acquisition mode, the battery life is around 43570 seconds, or 12 hours 6 minutes and 10 seconds.

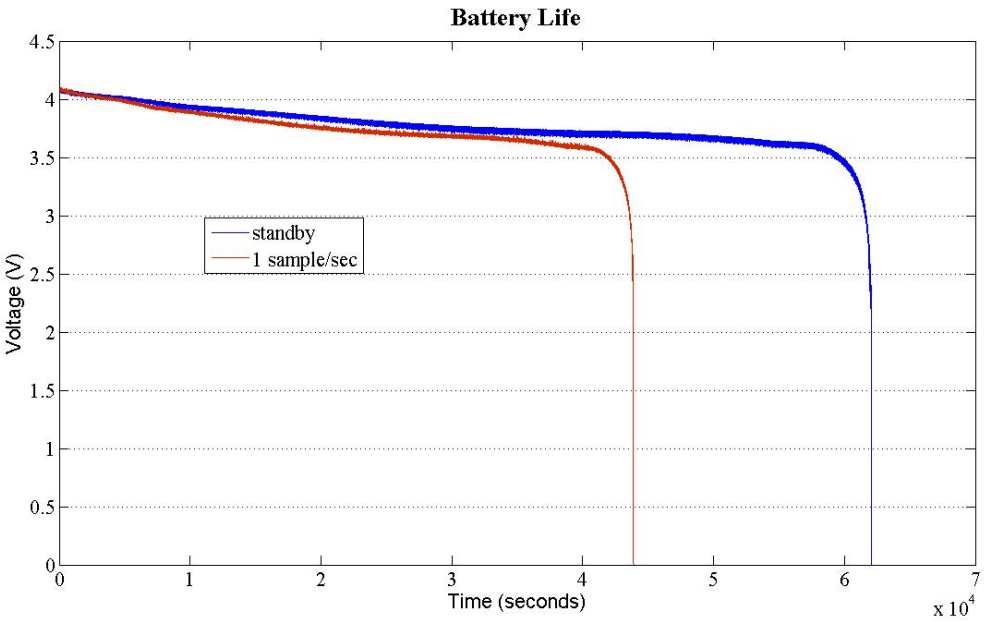

Fig.4.1. Graph of the Battery Life operating in 2 modes: in standby mode (blue) and acquiring 1 sample per second (red).

4.2. EBI Measurements

4.2.1. Resistance Measurements

To check the operational dynamic frequency range of the system, several known values of resistances have been tested. The chosen frequency range is the β-dispersion range, from around 10 kHz to 100 kHz. The main reasons are due to the limitation of the AD5933 to measure values below 5 kHz and also because of the most interesting dispersion in medical applications is β-dispersion, as mentioned in Chapter 2. Thus, two decades of resistance values, from 100Ω to 10kΩ, have been tested in 5 kHz-frequency steps after calibrating the system with a resistance value of 5100Ω. Table 4-I shows some of the obtained measurement values.

TABLE 4-I: MEASUREMENTS OF DIFFERENT RESISTANCES FOR SEVERAL FREQUENCIES.

Rth (Ω)	Frequency (Hz)						
	5000	10000	20000	40000	60000	80000	100000
100	475	478	478	473	469	465	459
150	492	494	495	490	487	485	480
270	551	554	556	553	548	545	542
360	600	603	605	599	596	591	592
430	640	643	646	642	638	636	633
510	705	710	712	710	710	712	712
620	818	823	826	824	824	825	825
750	930	936	939	937	936	937	936
820	1004	1009	1013	1010	1010	1010	1010
1000	1163	1170	1174	1171	1170	1171	1169
2200	2275	2283	2289	2284	2282	2284	2282
2700	2788	2795	2802	2794	2796	2792	2795
3300	3343	3357	3357	3357	3352	3352	3350
4300	4276	4298	4300	4292	4293	4283	4293
5100	5095	5101	5104	5109	5102	5103	5089
6200	6137	6154	6152	6129	6143	6142	6150
7500	7417	7365	7353	7349	7376	7388	7362
8200	7988	7946	7936	7916	7961	7925	7961
9100	8898	8902	8831	8841	8882	8885	8881
10000	9698	9715	9671	9729	9738	9683	9722

In Fig.4.2 an 'Estimated resistance vs. frequency' graph is shown. As it can be observed, every plot for every resistance value is completely flat, i.e constant. That means the estimated values, which have been acquired by the system, are independent on the frequency as expected from theory.

On the other hand, some problems can be observed. Firstly, for very low values of resistance the device exhibits a high error due to the design is not very accurate in this load range. Secondly, values below calibration resistance show a positive offset and values above calibration show a

negative one. This can be better observed in the Fig.4.3 where an 'expected value vs. theoretical value' plot is shown for several frequencies.

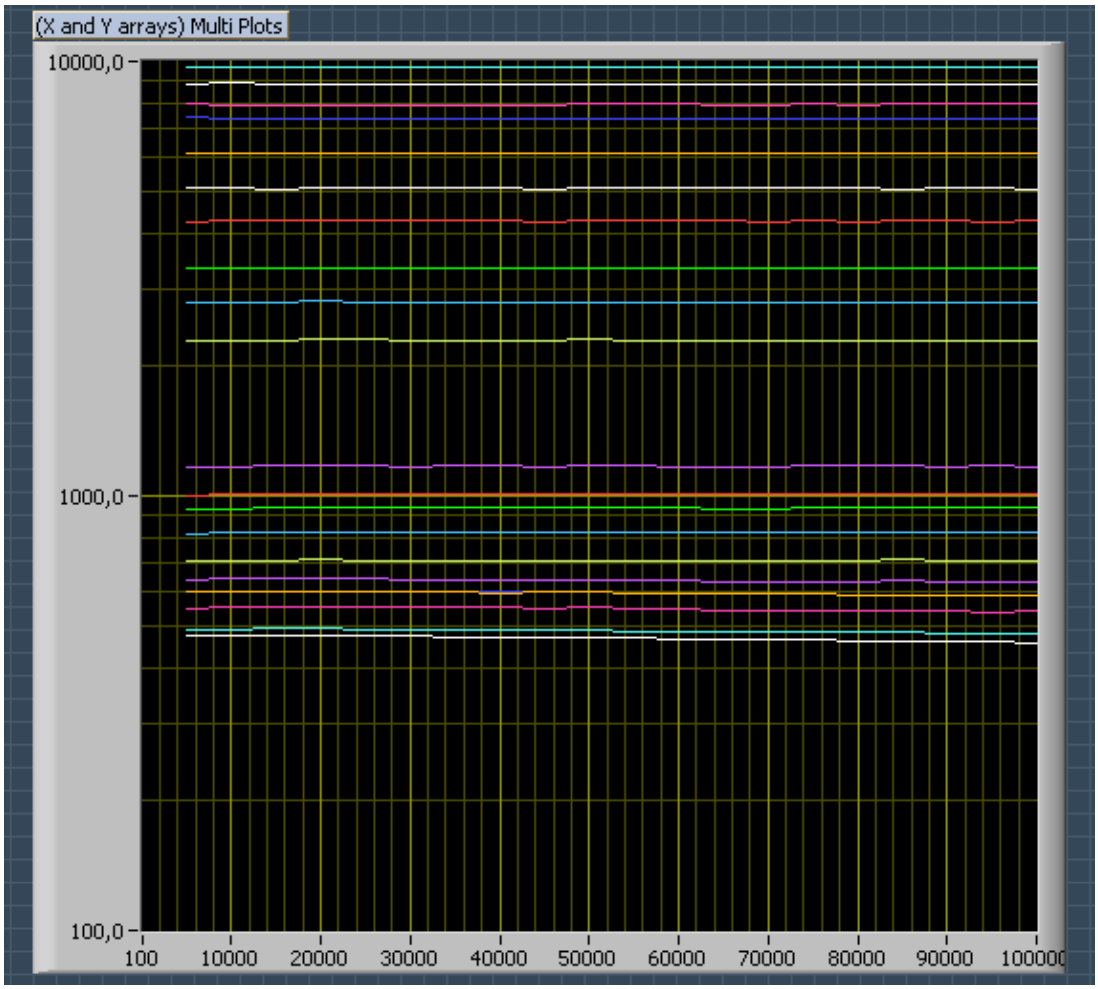

Fig.4.2. Resistance value vs. Frequency plot. Several resistances have been tested for the frequency range between 100Hz and 10 kHz in 5kHz-frequency steps.

Except at high values, a frequency-independence is observed along the tested range. Due to this fact, a software calibration is proposed to improve the results; see Fig.4.4.
This software calibration consists on applying the Equation (4.1). This equation is obtained calculating a regression line in the range between 500 Ω and 10kΩ at the frequency of 50 kHz.

$$Z\text{cal} = \left(Zmeas - 228.66\right)/0.9494 \qquad \textbf{Equation (4.1)}$$

Where Zmeas is the value obtained from AD5933 and Zcal is the calculated value applying the software calibration.

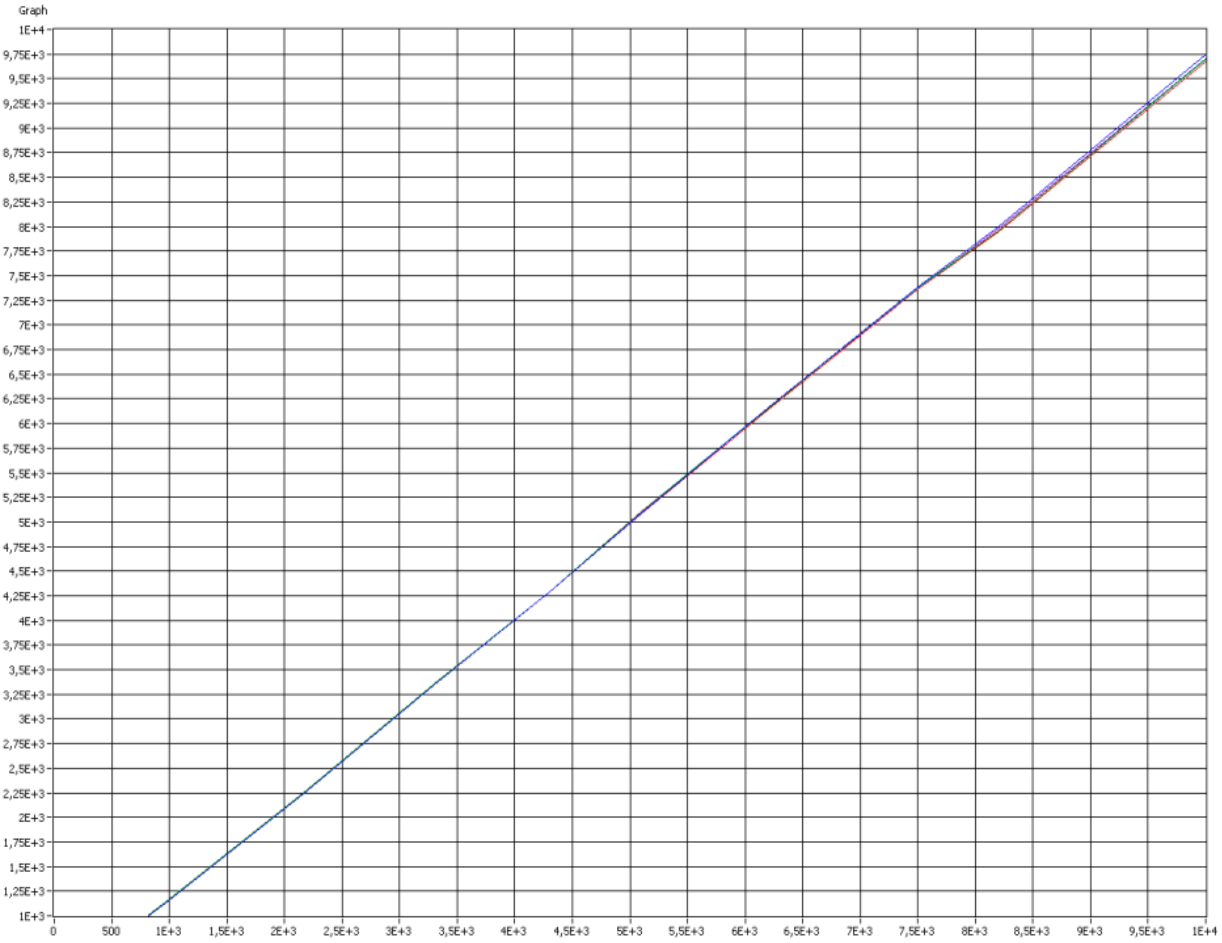

Fig.4.3. Theoretical Resistance vs. Measured Resistance for several frequencies: 5kHz, 25kHz, 50kHz, 75kHz and 100kHz. As observed, a frequency-dependence does not exist except of high values.

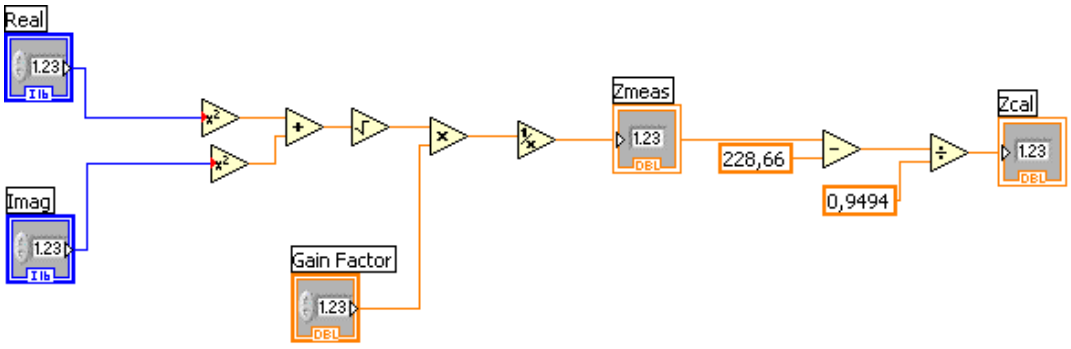

Fig.4.4. Software Calibration Block.

Table 4-II contains the compensated values for the same resistances and frequencies used in Table 4-I.

Table 4-III contains the errors with and without applying the calibration at 50 kHz are shown. As noticed, there is a high improvement using this calibration.

TABLE 4-II: ACQUIRED VALUES APPLYING THE SOFTWARE CALIBRATION.

Rth (Ω)	Frequency (Hz)						
	5000	10000	20000	40000	60000	80000	100000
100	259,47	262,63	262,63	257,36	253,15	248,94	242,62
150	277,38	279,48	280,54	275,27	272,11	270,00	264,74
270	339,52	342,68	344,79	341,63	336,36	333,20	330,04
360	391,13	394,29	396,40	390,08	386,92	381,65	382,70
430	433,26	436,42	439,58	435,37	431,16	429,05	425,89
510	501,73	506,99	509,10	506,99	506,99	509,10	509,10
620	620,75	626,02	629,18	627,07	627,07	628,12	628,12
750	738,72	745,04	748,20	746,09	745,04	746,09	745,04
820	816,66	821,93	826,14	822,98	822,98	822,98	822,98
1000	984,14	991,51	995,72	992,56	991,51	992,56	990,46
2200	2155,40	2163,83	2170,15	2164,88	2162,78	2164,88	2162,78
2700	2695,74	2703,12	2710,49	2702,06	2704,17	2699,96	2703,12
3300	3280,32	3295,07	3295,07	3295,07	3289,80	3289,80	3287,70
4300	4263,05	4286,22	4288,33	4279,90	4280,96	4270,42	4280,96
5100	5125,70	5132,02	5135,18	5140,45	5133,07	5134,13	5119,38
6200	6223,24	6241,14	6239,04	6214,81	6229,56	6228,50	6236,93
7500	7571,46	7516,68	7504,04	7499,83	7528,27	7540,91	7513,52
8200	8172,89	8128,65	8118,12	8097,05	8144,45	8106,53	8144,45
9100	9131,39	9135,60	9060,82	9071,35	9114,54	9117,70	9113,48
10000	9974,03	9991,93	9945,59	10006,68	10016,16	9958,23	9999,30

TABLE 4-III: ERROR WITH AND WITHOUT APPLYING THE SOFTWARE CALIBRATION AT 50 KHZ.

Rth (Ω)	Error (Zmeas-Rth)	
	Without Calibration	Calibration
100	373	157,36
150	340	125,27
270	282	70,57
360	240	31,13
430	213	6,42
510	202	-0,90
620	206	9,18
750	189	-1,80
820	192	5,09
1000	173	-5,33

Rth (Ω)	Error (Zmeas-Rth)	
	Without Calibration	Calibration
2200	87	-31,96
2700	99	7,33
3300	55	-7,04
4300	-6	-17,99
5100	5	36,23
6200	-51	35,88
7500	-123	29,32
8200	-240	-56,60
9100	-233	-1,26
10000	-278	-0,70

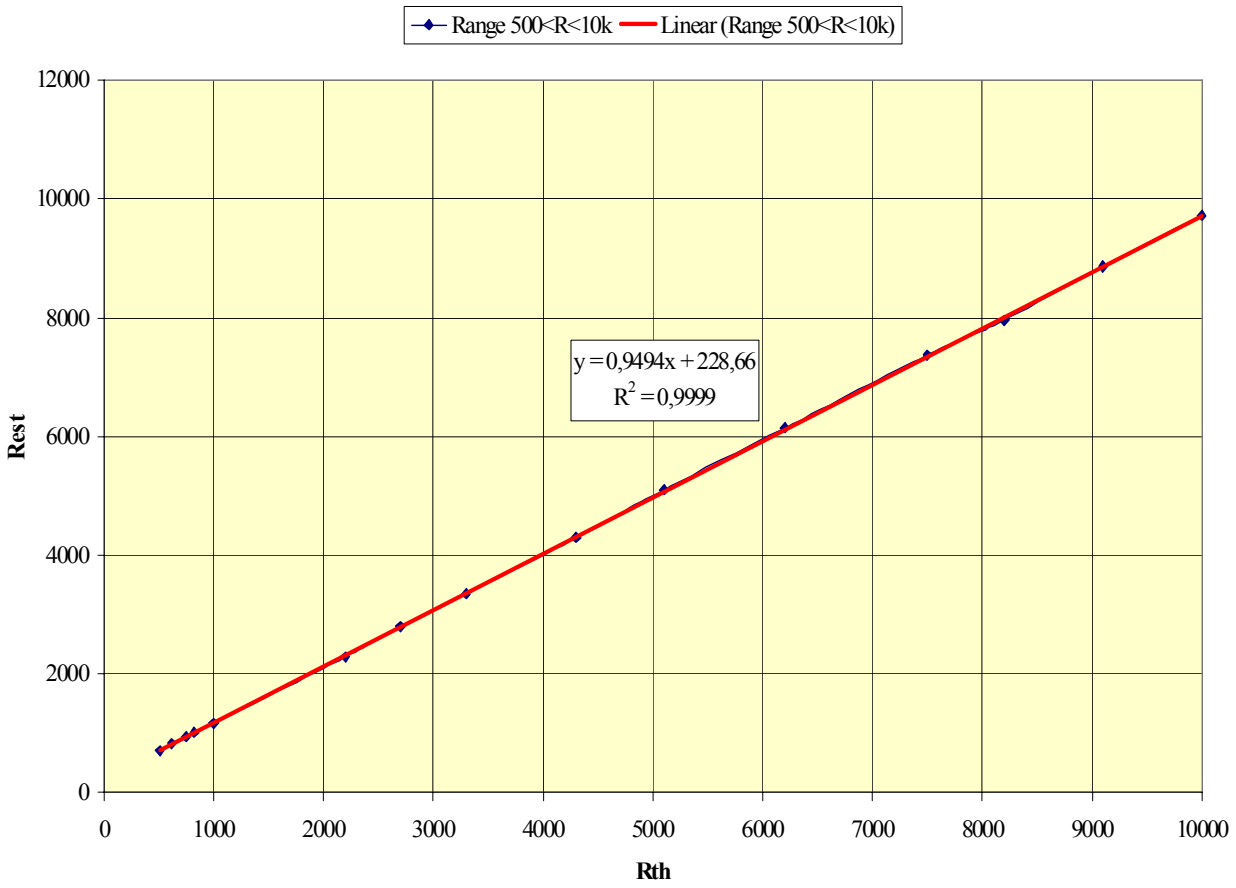

Fig.4.5. Tendency Line using a linear regression in the range between 500Ω and 10kΩ.

4.2.2. RC Circuit Topology Measurements

Two different circuit topologies have been chosen to test the performance of the measurement system obtaining the frequency response of a test load. In both cases, its phase and its magnitude were acquired and compared with the theoretical data, after applying the software calibration. As observed, the error in the measured phase is increased along the frequency reaching a maximum value of 5 degrees; see Fig.4.7 and Fig.4.9. On the other hand, the measured magnitude only shows a little error for small values of the frequency range; see Fig.4.6 and Fig.4.8.

The chosen topologies have been previously explained in Chapter 2 and they correspond with Fig.2.6 and Fig.2.4(c).

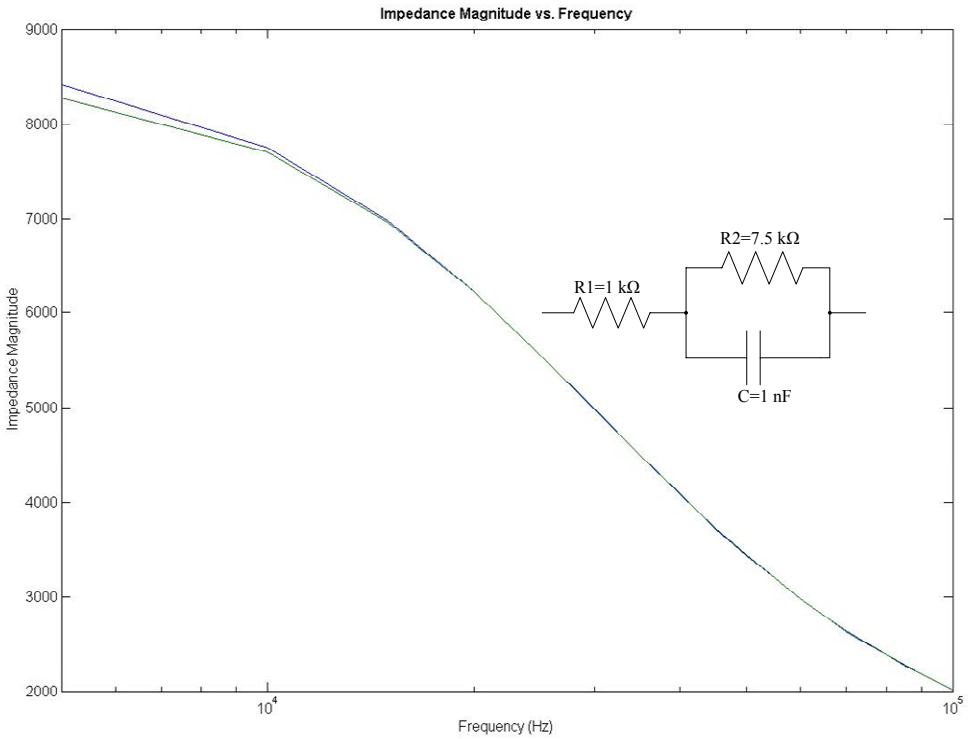

Fig.4.6. Impedance Magnitude vs. Frequency for a R1+R2//C topology. It corresponds with the topology shown in Fig.2.6 with R1=1k, R2=7k5 and C=1nF.

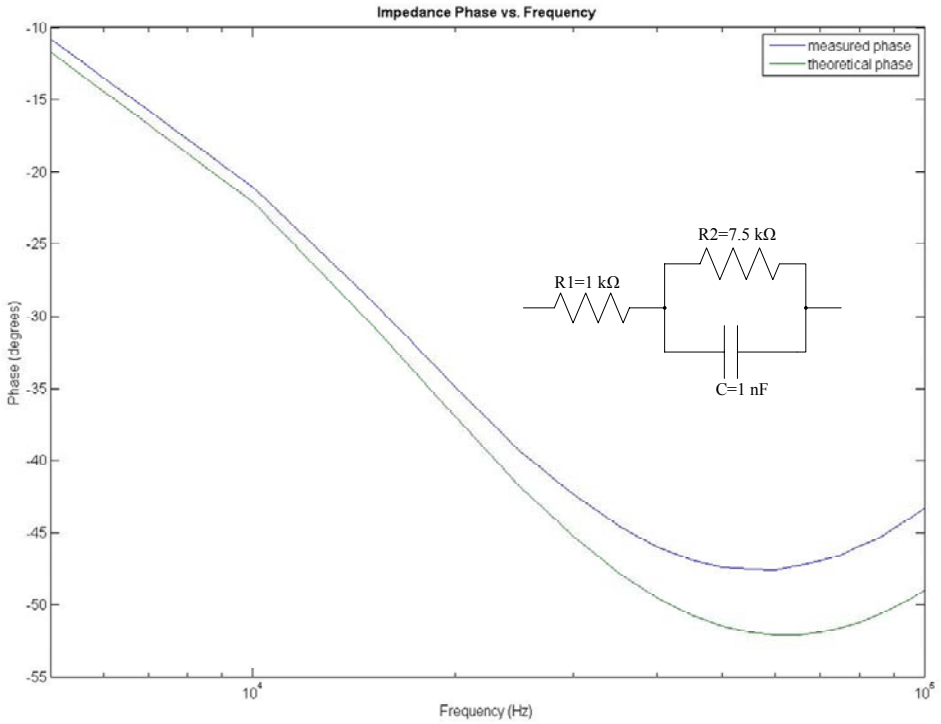

Fig.4.7. Impedance Phase vs. Frequency for a R1+R2//C topology. It corresponds with the topology shown in Fig.2.6 with R1=1k, R2=7k5 and C=1nF.

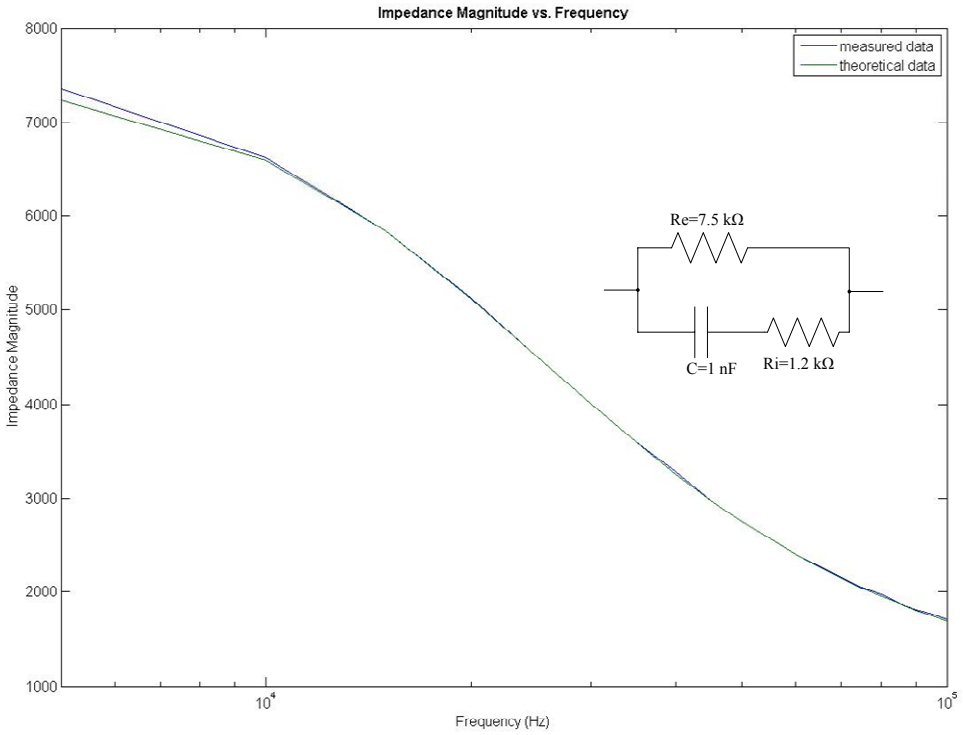

Fig.4.8. Impedance Magnitude vs. Frequency for a Re//(Ri+C) topology. It corresponds with the topology shown in Fig.2.4(c) with Re=7k5, Ri=1k2 and C=1nF.

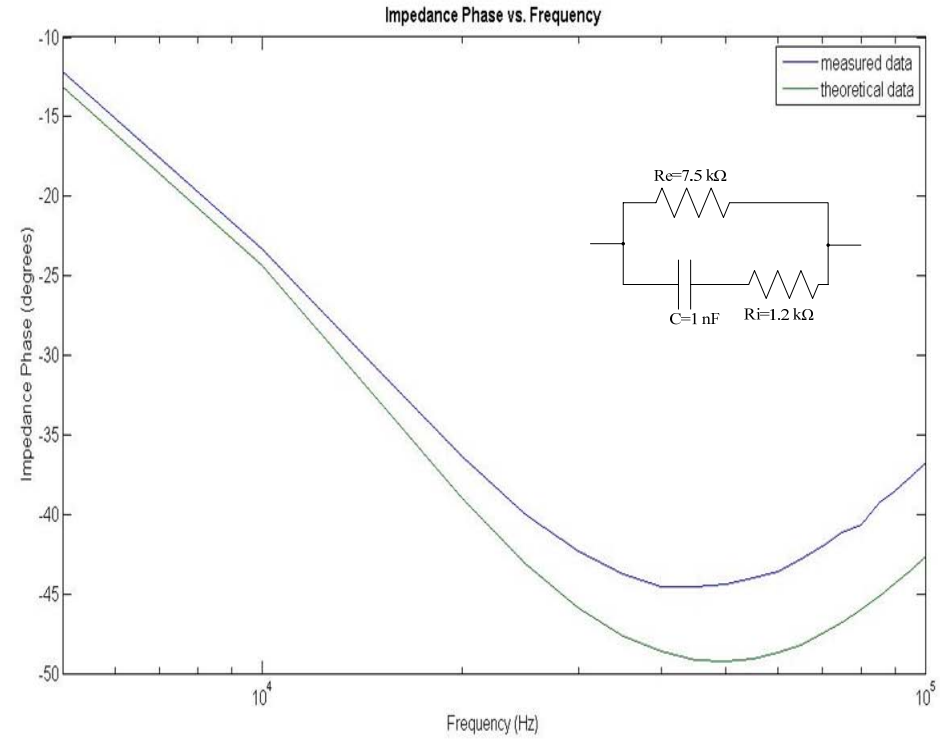

Fig.4.9. Impedance Phase vs. Frequency for a Re//(Ri+C) topology. It corresponds with the topology shown in Fig.2.4(c) with Re=7k5, Ri=1k2 and C=1nF.

4.2.3. Biological Measurements

To test the performance of the system measuring EBI, two kinds of measurements were taken. In thr first measurement, the EBI of a banana was measured along the frequency range between 5kHz and 100kHz. Both the obtained magnitude and phase are shown in Fig.4.10 (a) and (b), respectively. Since it is not possible to acquire data below 5kHz using the AD5933 without using a frequency divider, the magnitude plot starts in the slope and the maximum value cannot

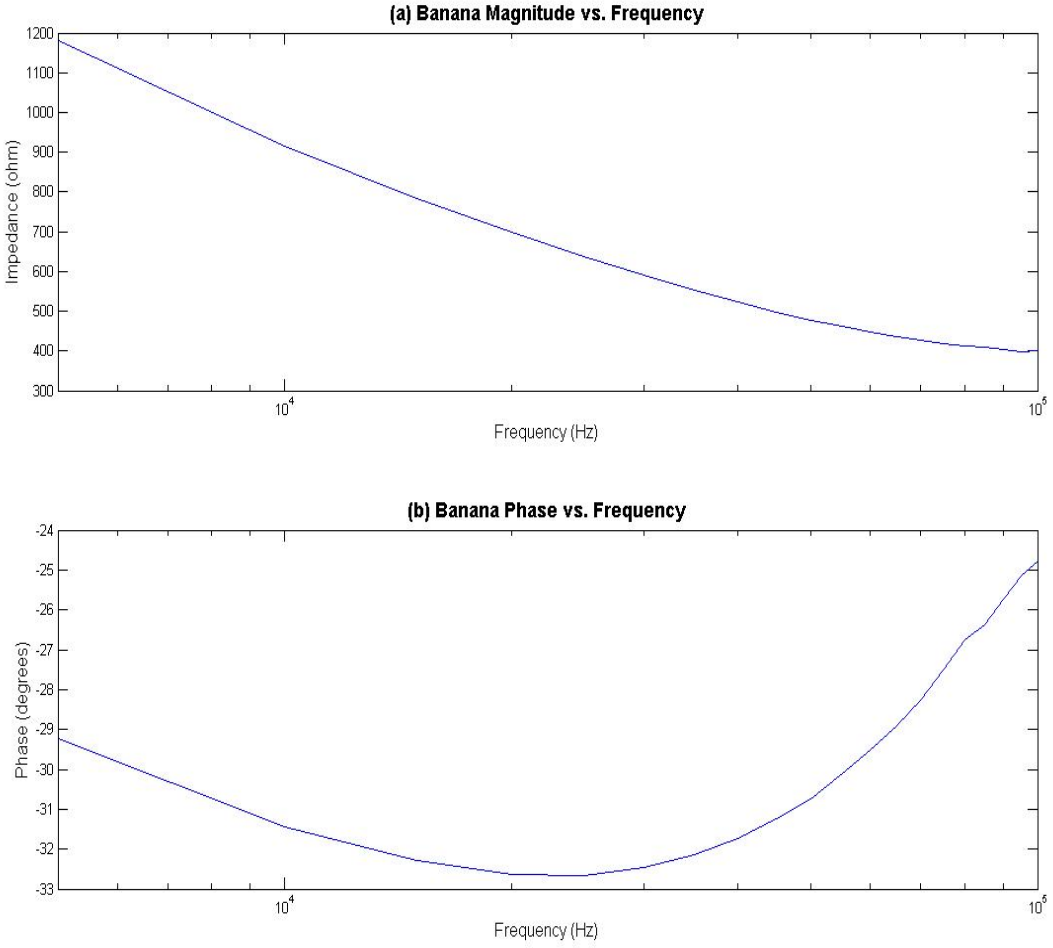

Fig.4.10. (a) Magnitude of a banana EBI along the β-dispersion range. (b) Phase of a banana EBI along the β-dispersion range. The start frequency is 5 kHz.

be observed. On the other hand, the phase plot shows how the minimum value is reached.
The second measurement consists on impedance pneumography. This method is used as a method for monitoring breathing. It consists on placing a surface electrode in each side of the thorax and measuring the variation of the impedance during inspirations and expirations. Usually and depending on the subject, on a base impedance of about 200 Ω, variations in the range of 2 Ω to 6 Ω can be observed in peak-to-peak amplitude for normal breathing. [18] [19]

Fig.4.11 shows an impedance pneumography acquired by the designed system. For safety reasons, these measurements were acquired using batteries as power sources to guarantee the isolation. In the figure, it can be observed as the base impedance is upper than 200 Ω and the peak-to peak amplitude is around 4 Ω as expected. The base impedance is higher due to our system is configured as a two-electrode system and the influence of the skin-electrode cannot be minimized as mentioned in Chapter 2.

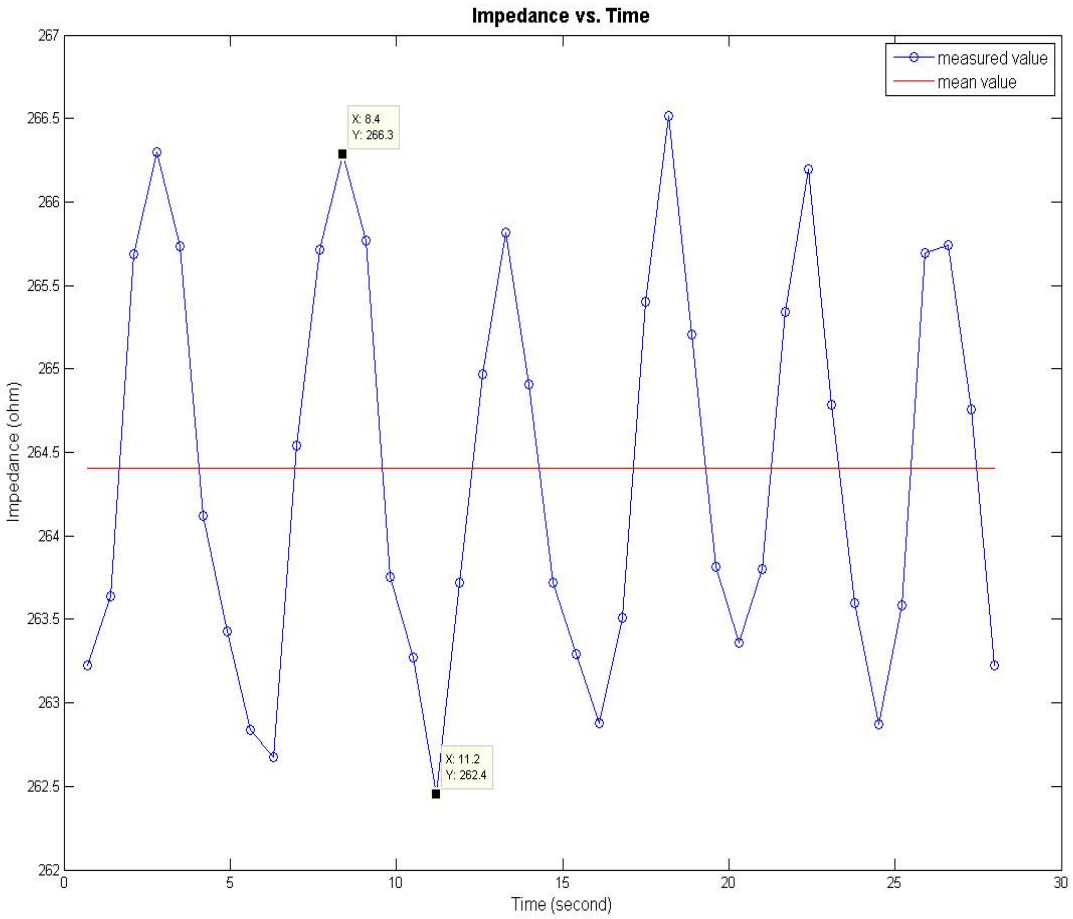

Fig.4.11. Impedance Pneumography. It shows a base impedance of 264.4 Ω and a peak-to-peak amplitude around 4 Ω.

4.3. Measurement Validation

4.3.1. Noise Influence in Measurements

To check how the measurements are influenced by noise, 500 samples of three different values of resistances (820Ω, 5100Ω and 8200Ω) were acquired for 2 different frequencies, 5kHz and

100kHz. Thus, applying the Matlab function called histfit(), an histogram with superimposed normal density is plotted for each data array; see Fig.4.12.

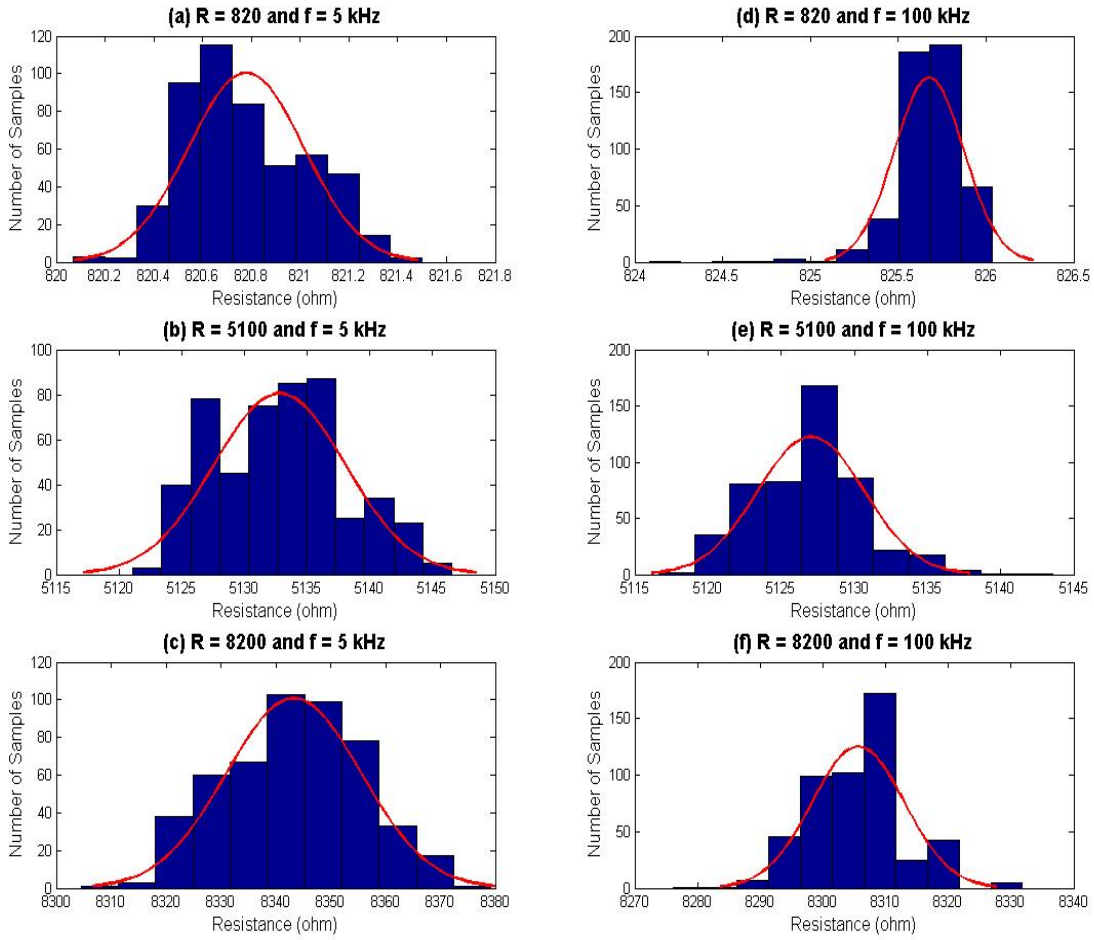

Fig.4.12. 500-sample histogram of several resistance values at two different frequencies. (a) Resistance of 820 Ω at 5 kHz. (b) Resistance of 5100 Ω at 5 kHz. (c) Resistance of 8200 Ω at 5 kHz. (d) Resistance of 820 Ω at 100 kHz. (e) Resistance of 5100 Ω at 100 kHz. (f) Resistance of 8200 Ω at 100 kHz.

Assuming that data act as a normal distribution, the made error is measured in the interval [μ-kσ, μ+kσ] where μ is the mean value of the data array, σ is the standard deviation of the data array and k is chosen for a p-value of 0.01 (k = 2.6); see Table 4-IV.

TABLE 4-IV: INTERVAL FOR A P-VALUE OF 1% AND THE ERROR FOR EACH IMPEDANCE VALUE FOR BOTH FREQUENCIES.

R (Ω)	Frequency = 5 kHz		R (Ω)	Frequency = 100 kHz	
	μ ± kσ k = 2.6	Error(%) =100*(kσ / μ)		μ ± kσ k = 2.6	Error(%) =100*(kσ / μ)
820	820.7 ± 0.6	0.07%	820	825.7 ± 0.5	0.06%
5100	5132.8 ± 13.6	0.26%	5100	5127.05 ± 9.4	0.18%
8200	8343.3 ± 31.8	0.38%	8200	8305.6 ± 19.0	0.23%

Thus, as the Table 4-IV shows, it can be assumed the measurements are not influenced severely by noise.

4.3.2. Temperature Influence in Measurements

To study the influence of the temperature, measurements on a carbon-film resistance with a reference value of 1kΩ were acquired during a period of time while the temperature changes approximately for 1ºC. Fig.4.15 shows a slight slope with a linear tendency. It can be observe a deviation of -0.86 Ω/ºC (or 860 ppm/ºC). Since this deviation is within the typical temperature coefficient range for this kind of resistances i.e. 1200 ppm/ºC, it can be concluded that the measurements acquired by the system are not significantly influenced by the temperature. Nevertheless, there is an apparent delay of 4 hours between the temperature and the observed resistance change.

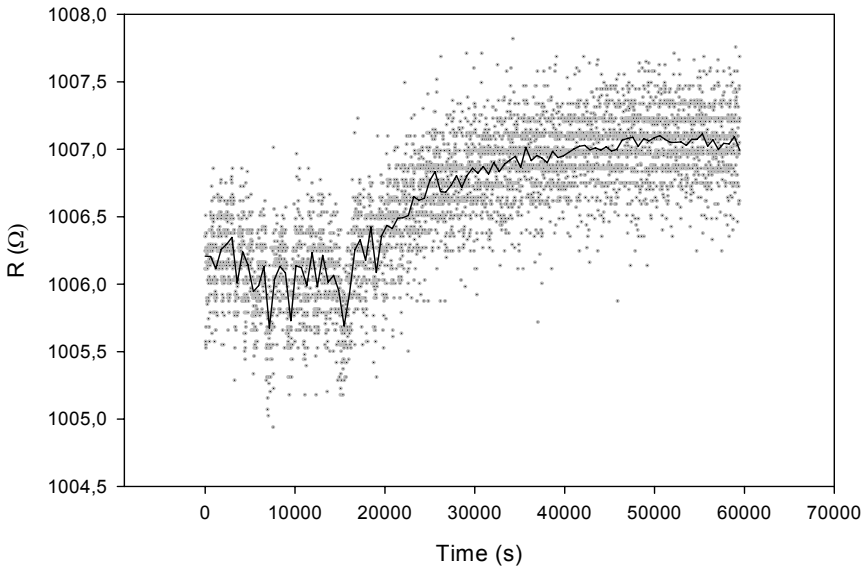

Fig.4.13. Time course of resistance measured along a 16 hours period.

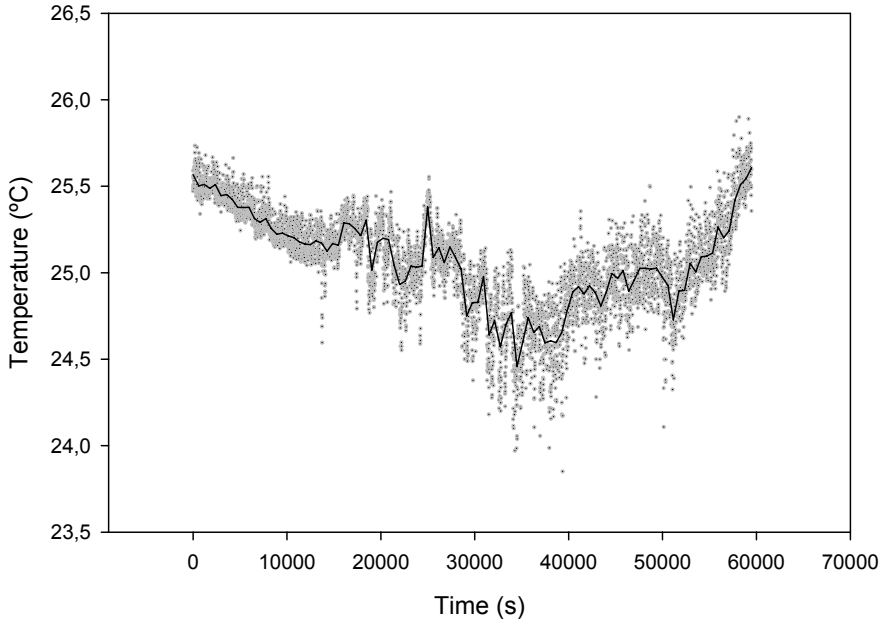

Fig.4.14. The time course of temperature measured along a 16 hours period with a temperature change of approximately 1ºC.

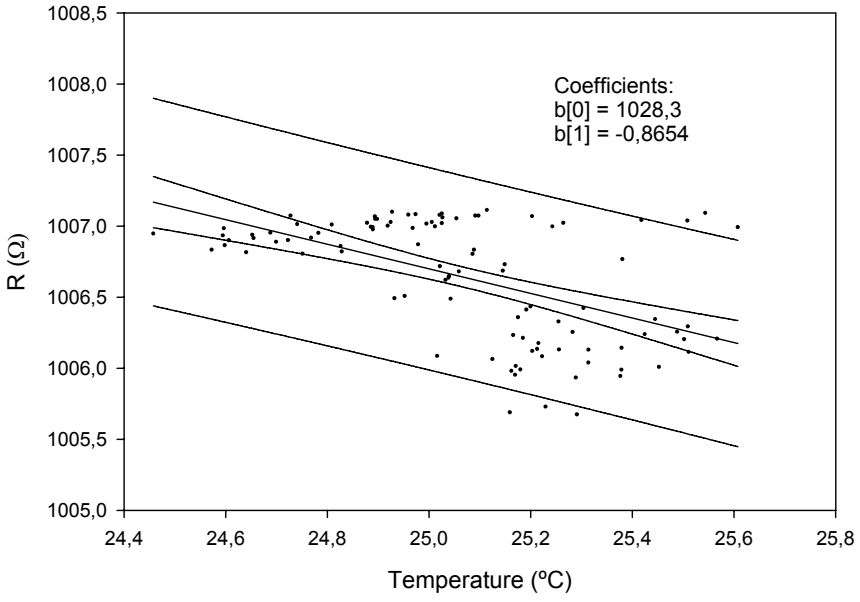

Fig.4.15. Impedance vs. Temperature Plot. A light tendency in the measurements can be observed due to temperature changes.

CHAPTER 5

CONCLUSIONS & FUTURE WORK

5.1 General Conclusions

After implementing and evaluating the designed system, several conclusions were taken according to some features as a WMD circuit:

- *Small & Lightweight*: As mentioned in Chapter 2, a WMD needs to be minimized due to volume/weight restrictions. As the implemented system was built using SMDs, the volume/weight restrictions depend on the volume/weight of the battery. While the board size is 7.5cm x 5.3cm x 0.2cm, the battery is 6.4cm x 3.6cm x 0.5cm. Hence, if a smaller and lighter device is required, the current battery should be replaced by a smaller and lighter one.
- *Low power*: A stand-alone power supply of minimum 15 hours without recharging is mandatory for WMD, as mentioned in Chapter 2. In Chapter 4, Fig.4.1 showed as the battery life is in the range between 12 hours (continuously acquiring) and 17 hours (standby mode). As noticed, there is not a high difference in terms of battery life depending on which mode the system is. This is because of the inductance used in the PMB; see Fig.3.2. Due to the On/Off Logic Control of the MAX1763 IC is not used and this Step-Up is always turned on, the battery continues discharging through the inductance although the EBI block remains in Standby mode. Thus, although the battery life can be enough in this first prototype, it should be improved for newer prototypes due to more blocks, such as wireless communication block, can be added in a recent future.

As regards the EBI block, although the acquired measurements are quite fitted according to the theoretical values, some limitations of the AD5933 were noticed:

- *Measurement Configuration*: Due to AD5933 is a two-electrode impedance measurement system, the acquired EBI measurements also contain the electrode-skin impedance limiting the range of applications where AD5933 can be used.
- *Safety*: Due to the voltage output contains a dc level which is different from the dc level at V_{in}, an imbalance is produced and a dc voltage flows across the electrodes and the tissue-under-study (TUS) which can be a health hazard for the patient. Furthermore, as the AD5933 has no control over the injected current, the limits set by IEC-60601 migth be accomplished.
- *Load Limitations*: As the maximum current limit of AD5933 is 5.8 mA at range 1 (the voltage source supplies around 1.9 Vpp), the minimum impedance value which can be measured is 160 Ω approximately. For values below this limit, the AD5933 output pin would be saturated and the acquired results would be wrong. This might not be a limitation in practice because of the electrodes increase the value of the load in EBI applications.

❖ *Accuracy*: The accuracy of the system depends on the value of the feedback resistor setting between RFB and VIN pins. As mentioned in Chapter 3, to improve its accuracy and to get the ADC works in the linear region, the total gain of the feedback should be as close as possible to the unity gain. To accomplish this, the feedback resistor should be as close as possible to the value of the TUS impedance but due to this value is unknown, it is important to fit the working range as much as possible.

5.2. Future work

To solve and to improve this first version of this WMD, two general ideas are explained as a future work lines.

5.2.1. Front-End

To solve the limitations found on the EBI block, an analog front-end is proposed. Adding very few ICs and a few passive components to the designed EBI block, a complete four-electrode measurement system can be implemented. As reference, the AFE implemented by [20] can be used; see Fig.5.1. Through this AFE, the safety, accuracy and load limitations are improved and it adapts AD5933 for EBI measurements in patients remaining practically the same size.

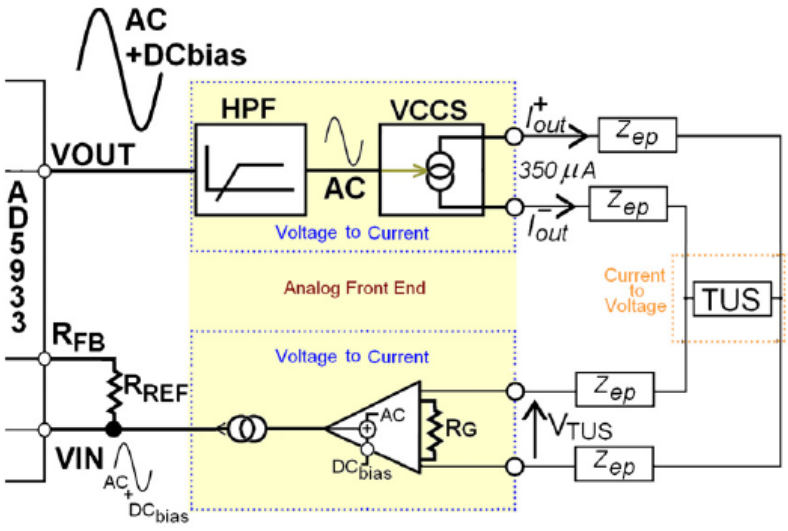

Fig.5.1. Functional block diagram of the proposed AFE.

5.2.2. Embedded System

To improve the power management and the portability of the system, the use of a microcontroller (μC) is proposed to monitor both blocks of the system. This μC should be a low-power one to extend the battery life as much as possible. Furthermore, an I2C module is required too. Therefore, the NI USB/I2C interface would not be needed and the Labview application could be replaced by a C-programming code. Thus the portability, and also the use of the memory space, would be improved. Moreover, other blocks could be added and controlled through this μC such as a Bluetooth module which would remove the use of communication wires.

REFERENCES

[1] Seoane F 2007 Electrical Bioimpedance Cerebral Monitoring: Fundamental Steps towards Clinical Application. In: *Signal & Systems,* (Göteborg: Chalmers University of Technology) p 154

[2] MesserWoland and Szczepan1990 2006 Biological_cell.svg available at: http://en.wikipedia.org/wiki/File:Biological_cell.svg[1]

[3] Definition of Electrolyte. Available at: http://www.medterms.com

[4] Rompaey L V 2008 Plasmamembraan.jpg. Available at: http://commons.wikimedia.org/[2]

[5] Grimnes S and Martinsen O G 2005 Cole electrical impedance Model-a critique and an alternative IEEE Transactions on Biomedical Engineering 52 132-5

[6] U.Kyle, I.Bosaeus, Lorenzo A D, P.Deurenberg, M.Elia, J.Gómez, B.Heitmann, L.Kent-Smith, J.Melchior and M.Pirlich 2004 Bioelectrical impedance analysis—part I: review of principles and methods Clinical Nutrition 23 1226-43

[7] Figure available at: http://www.rowett.ac.uk/edu_web/index.html

[8] Bio-Impedance Analysis definition. Available at: http://www.longevityhealthcenter.com

[9] Bio-Impedance Analysis definition. Available at: http://florey.biosci.uq.edu.au/BIA/

[10] Bio-Impedance Analysis definition. Available at: http://www.biospaceamerica.com/bia/

[1] This image is under CC-BY-SA (Creative Commons Attribution and Share Alike license) and GFDL (GNU Free Documentation License) licenses. See GFDL conditions at http://en.wikipedia.org/wiki/GNU_Free_Documentation_License.
[2] This image is under CC-BY-SA license.

[11] Grimnes S and Martinsen Ø G 2000 Bioimpedance & Bioelectricity Basics: Academic Press)

[12] Ibáñez Soria D 2008 Implementation of an Electrical Bioimpedance Monitoring System and a Tool for Bioimpedance Vector Analysis. University College of Boras) p 85

[13] Scheffer M and Hirt E 2004 Wearable devices for emerging healthcare applications. In: Proceedings of the 26th Annual International Conference of the IEEE EMBS, (San Francisco, CA, USA pp 3301-4

[14] Gentile K, Brandon D and Harris T 2003 Direct Digital Synthesis Primer. (Analog Devices)

[15] Matousek T Inter Integrated Circuits bus by Philips Semiconductors.

[16] Definition of I2C. Available at: http://en.wikipedia.org/wiki/I2c

[17] Information of I2C. Available at: http://www.dnatechindia.com

[18] Brown B H, Smallwood R H, Barber D C, Lawford P V and Hose D R 1999 Medical Physics and Biomedical Engineering. CRC Press) p 736

[19] Rosell J and Webster J G 1995 Signal-to-Motion Artifact Ratio Versus Frequency for Impedance Pneumography IEEE Transactions on Biomedical Engineering 42 321-3

[20] Seoane F, Ferreira J, Sánchez J J and Bragós R 2008 An analog front-end enables electrical impedance spectroscopy system on-chip for biomedical applications Physiological Measurements 29 267-78

[21] Blanco D 2008 Development of a Software Tool for Electrical Bioimpedance Spectroscopy Analysis University College of Boras) p 72

[22] MAXIM Datasheets available at: http://www.maxim-ic.com/

[23] Analog Devices Datasheets available at: http://www.analog.com/en/index.html

APPENDIX A

ORCAD SCHEMATICS

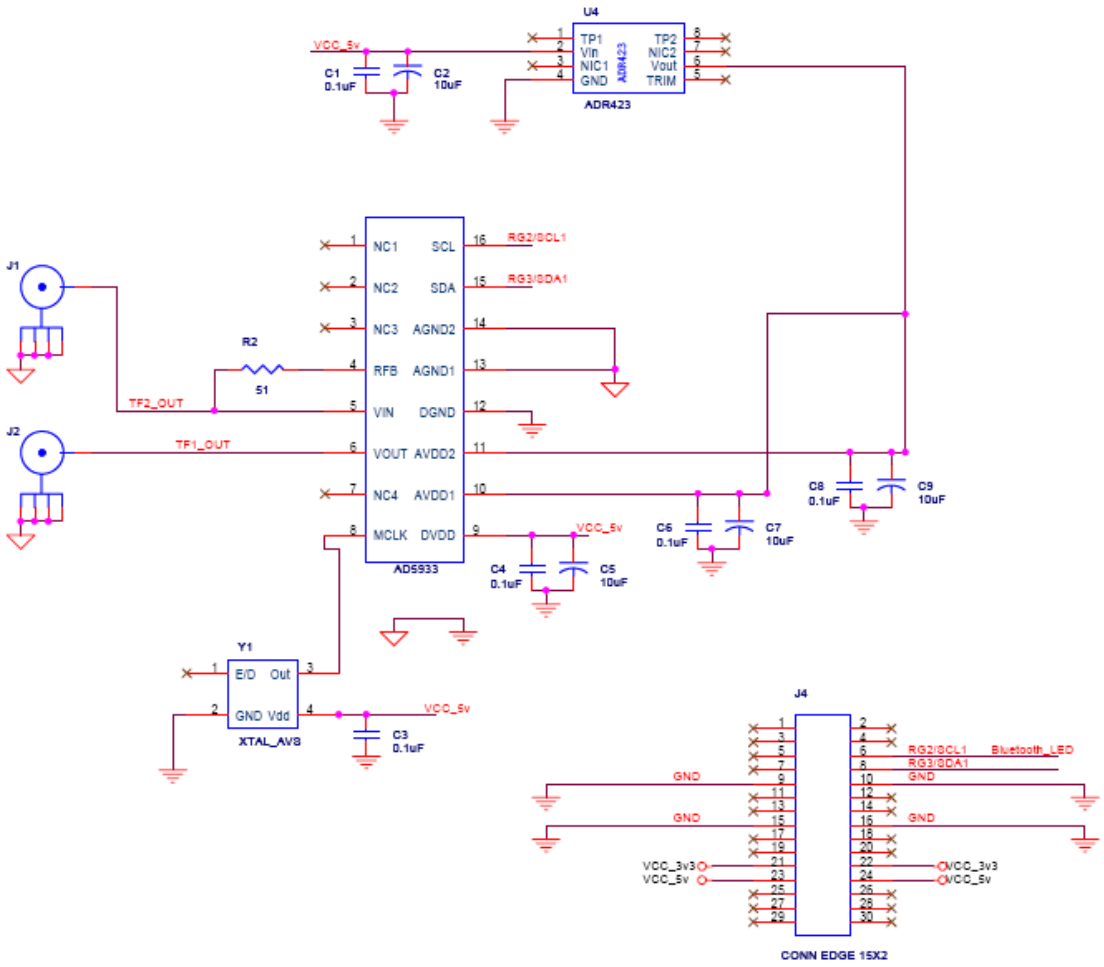

Fig.A.1. Scheme of the Electrical Bioimpedance Measurement Block.

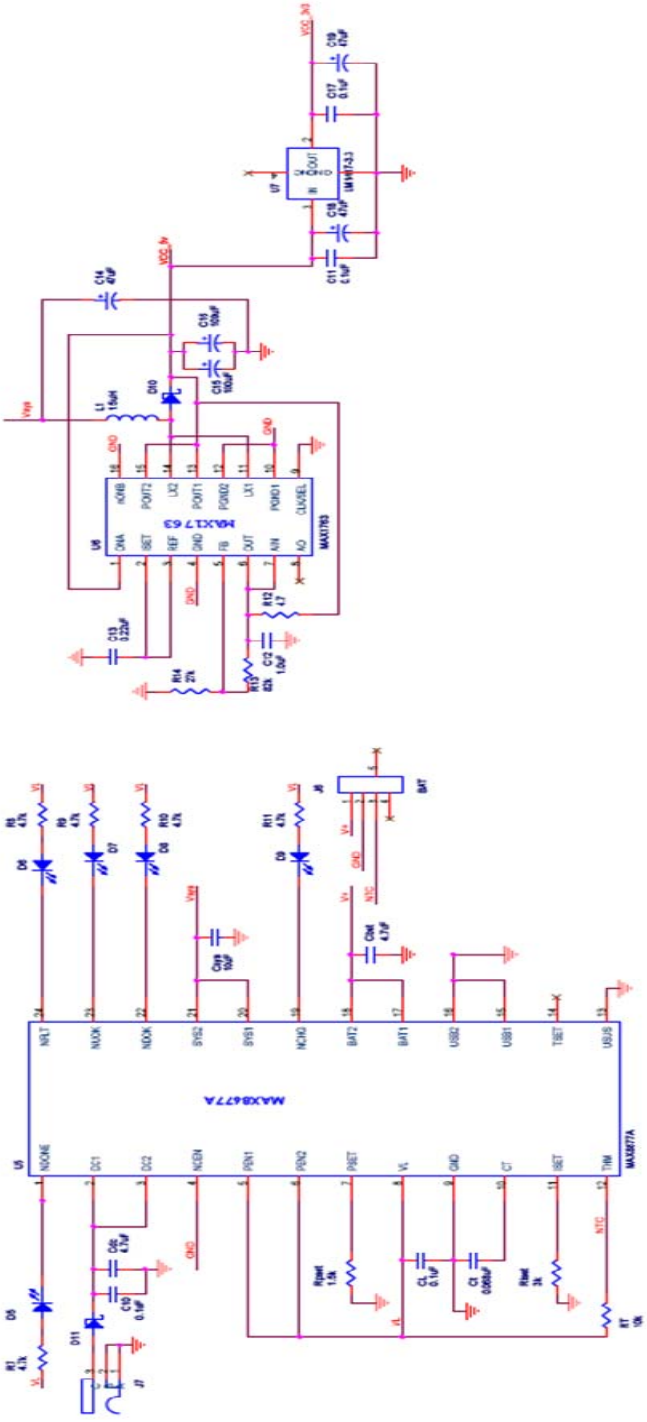

Fig.A.2. Scheme of the Power Management Block.

APPENDIX B

LAYOUT

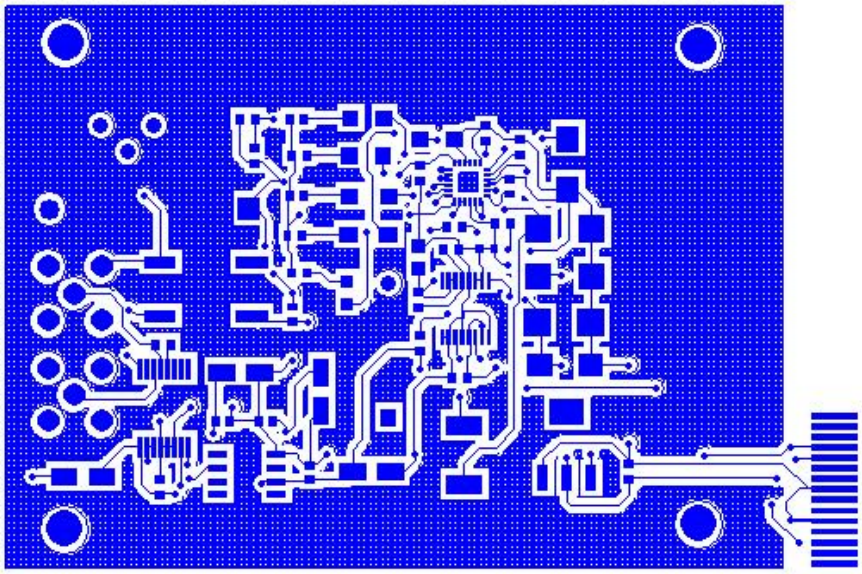

Fig.B.1. Top Layer.

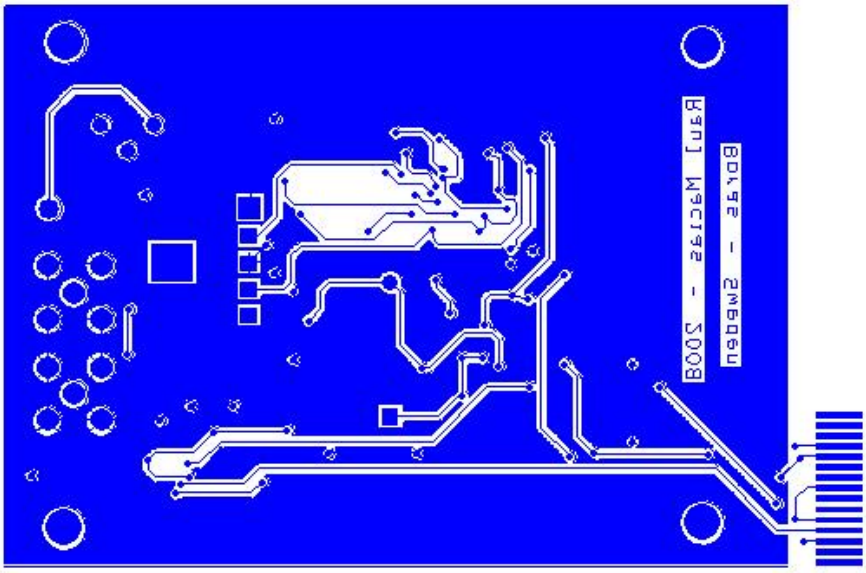

Fig.B.2. Botton Layer.

APPENDIX C

LABVIEW BLOCKS

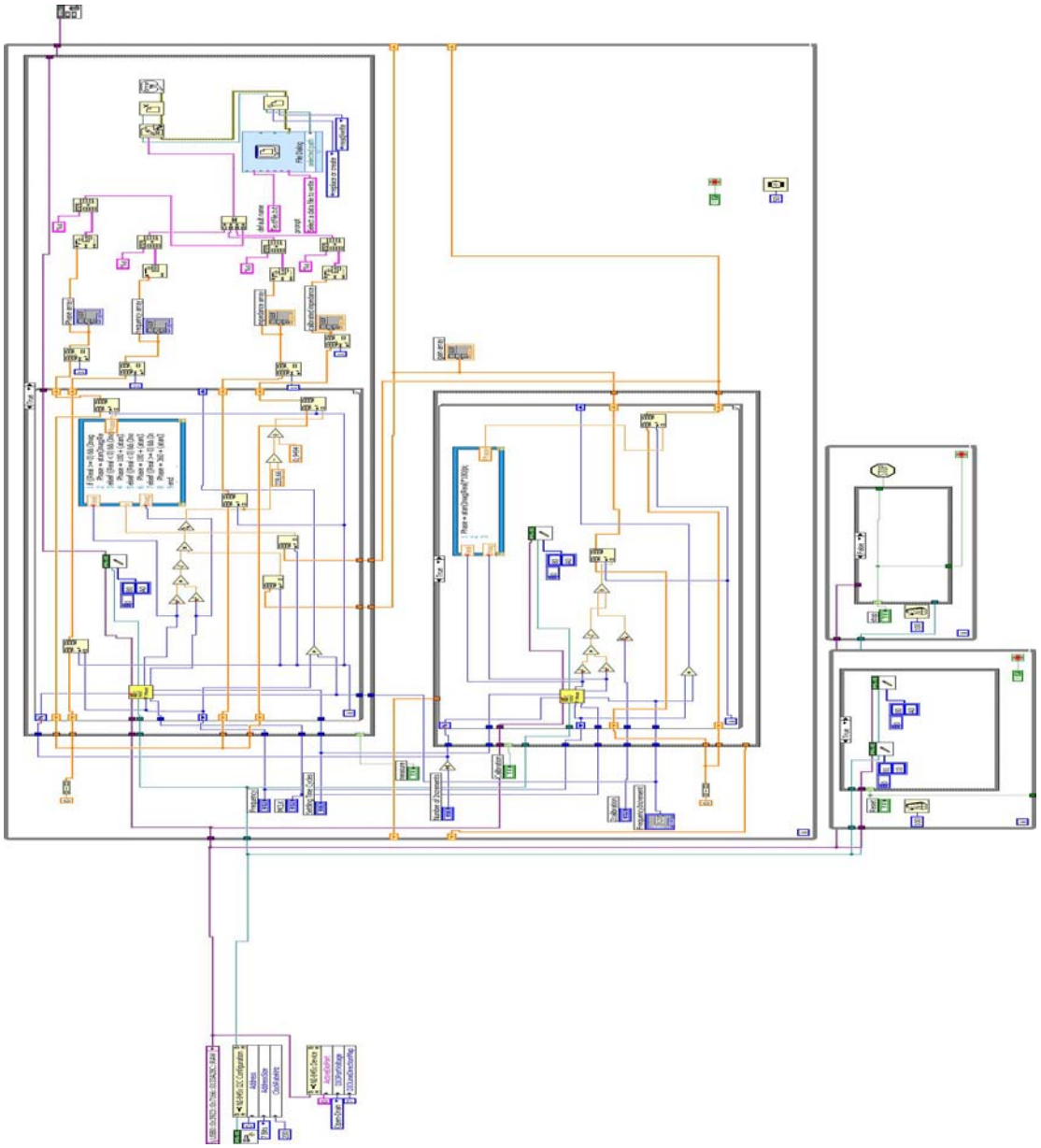

Fig.C.1. Block diagram to measure impedance magnitude & phase.

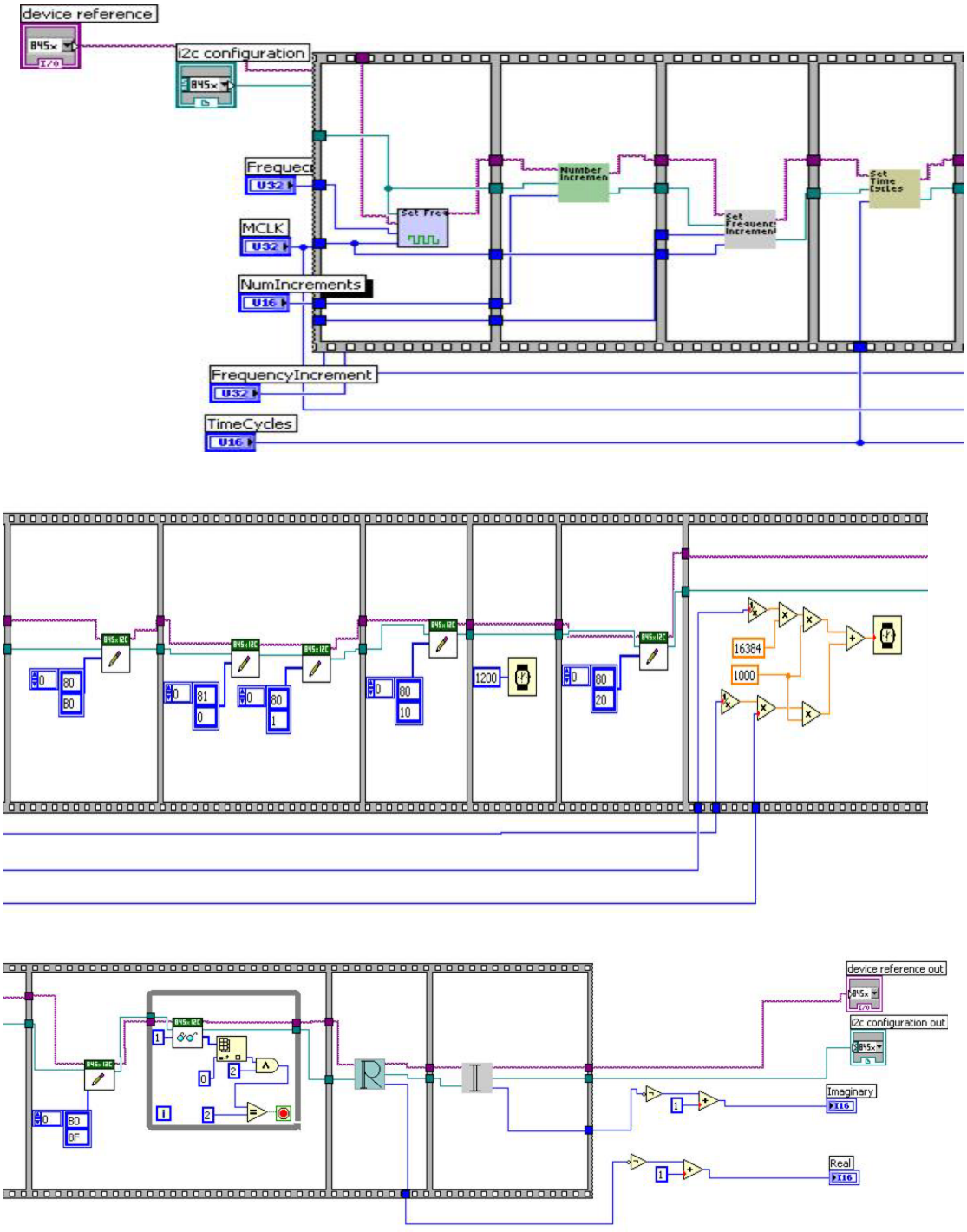

Fig.C.2. Block diagram of the FreqMeas VI.

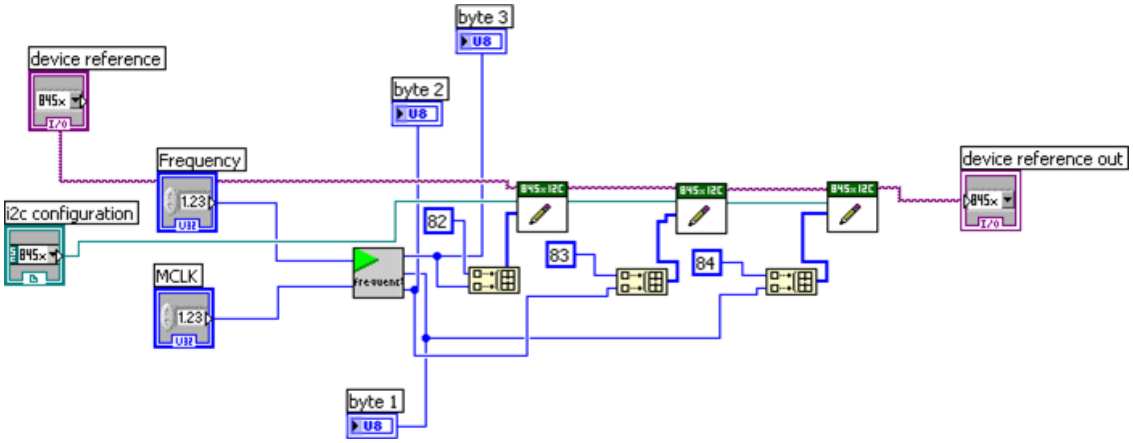

Fig.C.3. Block diagram of the SetFreq VI.

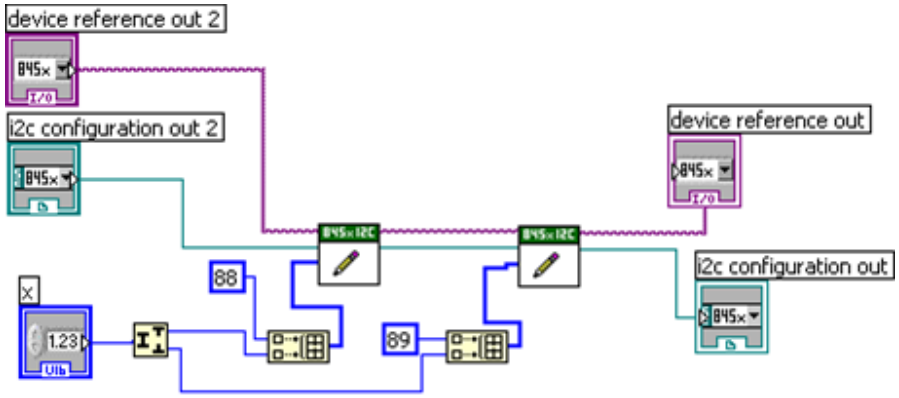

Fig.C.4. Block diagram of the NumberIncrement VI.

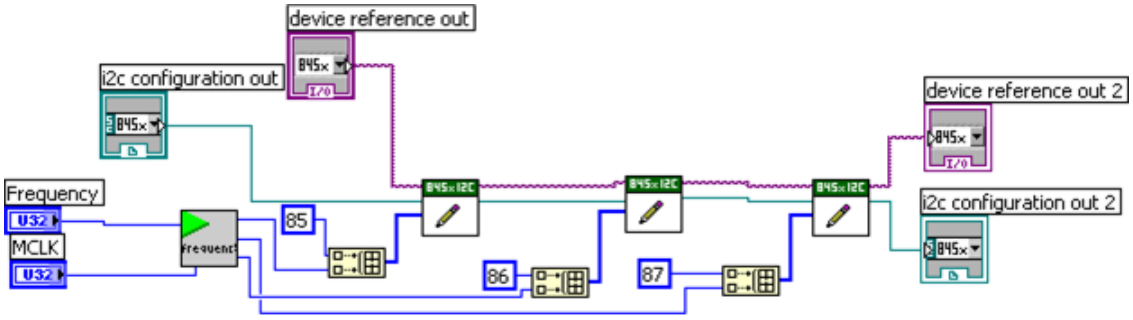

Fig.C.5. Block diagram of the SetFrequencyIncrement VI.

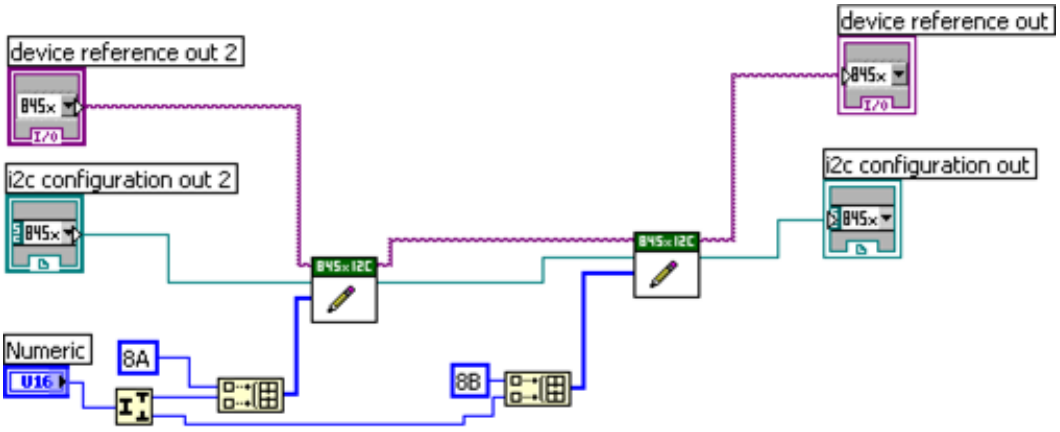

Fig.C.6. Block diagram of the SetTimeCycles VI.

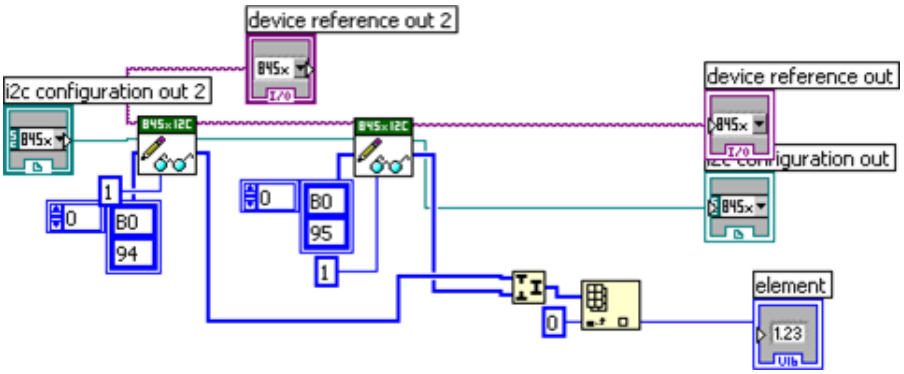

Fig.C.7. Block diagram of the Read-Real VI.

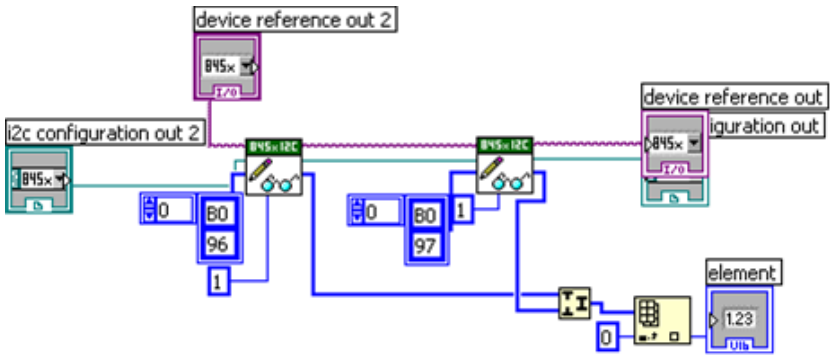

Fig.C.8. Block diagram of the Read-Imaginary VI.